Interaction between the autophagy protein Beclin 1 and Na^+,K^+-ATPase during starvation, exercise and ischemia

Álvaro F. Fernández[1,2], Yang Liu[1,2], Vanessa Ginet[3], Mingjun Shi[4], Jihoon Nah[5], Zhongju Zou[1,2,6], Anwu Zhou[7], Bruce A. Posner[7], Guanghua Xiao[8], Marion Tanguy[9,10], Valérie Paradis[9,11], Junichi Sadoshima[5], Pierre-Emmanuel Rautou[9,10], Julien Puyal[3], Ming Chang Hu[2,4] and Beth Levine[1,2,6,*]

[1]Center for Autophagy Research,
[2]Department of Internal Medicine, University of Texas Southwestern Medical Center, Dallas, Texas, USA.
[3]Department of Fundamental Neurosciences, University of Lausanne, Lausanne, Switzerland.
[4]Charles and Jane Pak Center for Mineral Metabolism and Clinical Research, University of Texas Southwestern Medical Center, Dallas, Texas, USA.
[5]Department of Cell Biology and Molecular Medicine, Cardiovascular Research Institute, Rutgers New Jersey Medical School, Newark, New Jersey, USA.
[6]Howard Hughes Medical Institute,
[7]Department of Biochemistry,
[8]Department of Clinical Sciences, University of Texas Southwestern Medical Center, Dallas, Texas, USA.
[9]Université de Paris, Centre de recherche sur l'inflammation, Inserm, Paris, France
[10]Service d'Hépatologie, DHU Unity, Pôle des Maladies de l'Appareil Digestif, Hôpital Beaujon, AP-HP, Clichy, France
[11]Service d'anatomie pathologique, Hôpital Beaujon, AP-HP, Clichy, France

*Correspondence:
Beth Levine, M.D.
Howard Hughes Medical Institute
Professor of Internal Medicine and Microbiology
Charles Cameron Sprague Distinguished Chair in Biomedical Science
Director, Center for Autophagy Research
UT Southwestern Medical Center
5323 Harry Hines Blvd.
Dallas, Texas 75390-9113
Tel. 214-648-0493
Fax. 214-648-0284
E-mail: beth.levine@utsouthwestern.edu

Conflict of interest: B.L. is a scientific co-founder of Casma Therapeutics, Inc.

Abstract

Autosis is a distinct form of cell death that requires both autophagy genes and the Na^+,K^+-ATPase pump. However, the relationship between the autophagy machinery and Na^+,K^+-ATPase is unknown. We explored the hypothesis that Na^+,K^+-ATPase interacts with the autophagy protein Beclin 1 during stress and autosis-inducing conditions. Starvation increased the Beclin 1/Na^+,K^+-ATPase interaction in cultured cells, and this was blocked by cardiac glycosides, inhibitors of Na^+,K^+-ATPase. Increases in Beclin 1/Na^+,K^+-ATPase interaction were also observed in tissues from starved mice, livers of patients with anorexia nervosa, brains of neonatal rats subjected to cerebral hypoxia-ischemia (HI) and kidneys of mice subjected to renal ischemia reperfusion injury (IRI). Cardiac glycosides blocked the increased Beclin 1/Na^+,K^+-ATPase interaction during cerebral HI injury and renal IRI. In the mouse IRI model, cardiac glycosides reduced numbers of autotic cells in the kidney and improved clinical outcome. Moreover, blockade of endogenous cardiac glycosides increased Beclin 1/Na^+,K^+-ATPase interaction and autotic cell death in mouse heart during exercise. Thus, Beclin 1/Na^+,K^+-ATPase interaction is increased in stress conditions, and cardiac glycosides decrease this interaction and autosis in both pathophysiological and physiological settings. This cross-talk between cellular machinery that generates and consumes energy during stress may represent a fundamental homeostatic mechanism.

Introduction

Eukaryotic cells are constantly exposed to different types of both extracellular and intracellular stress. To counteract such stress and maintain cellular homeostasis, cells trigger a tightly regulated network of pro-survival responses that includes autophagy (1). Autophagy is an evolutionarily conserved pathway that mediates the transport of cytosolic components to the lysosome for degradation (2). Through this catabolic process, cells can survive a wide range of insults. For example, during energy deprivation, autophagy mediates the mobilization of different cellular energy stores, such as lipids or glycogen, providing a cell-autonomous mechanism for ATP generation (3). However, high levels of autophagy that occur during severe stress, especially tissue ischemia, can also be detrimental for the cell, leading to its death (4). The concept of "autophagic cell death" describes different types of cell death that typically exhibit massive formation of autophagic vacuoles and that are dependent on autophagy genes (4, 5).

Our group previously described autosis, a specific type of autophagic cell death that shows distinctive ultrastructural features, including increased substrate adhesion and expansion of the perinuclear space (6). This unique pathway has been described under different stress conditions in vitro and in vivo (7-9), including in the livers of patients with severe anorexia nervosa (7) and a rat model of perinatal cerebral hypoxia-ischemia (6, 10). A growing number of studies suggest a dual role for autophagy in ischemia in different organs (11-15), with autophagy-dependent cell death partially contributing to adverse clinical outcomes (4, 16-19). However, the precise determinants of whether autophagy is detrimental during ischemic injury remain unclear. It is interesting to speculate that additional molecules may interface with the autophagy pathway, thereby regulating its switch from a protective process to a death pathway and providing potential therapeutic targets in ischemic disease.

Although the precise molecular mechanisms of autosis remain unknown, this pathway requires Na^+,K^+-ATPase (6). Genetic silencing of Na^+,K^+-ATPase or pharmacological inhibition of Na^+,K^+-ATPase by cardiac glycosides, natural inhibitors of Na^+,K^+-ATPase (20), blocks autosis in vitro and the cardiac glycoside, neriifolin, decreases autosis and cerebral infarct size in a rat model of cerebral hypoxic-ischemic (HI) injury. Na^+,K^+-ATPase is a pump that is responsible for the ATP-dependent exchange of Na^+ and K^+ ions across membranes (21). Na^+,K^+-ATPase is also involved in the import of protons (22) and the initiation of different signaling pathways (23). Interestingly, Na^+,K^+-ATPase activity is markedly reduced during hypoxia or a single bout of exercise (24), and endogenous cardiac glycosides (synthesized by the adrenal gland and hypothalamus) are released into the circulation in such settings (25). These studies suggest the existence of a systemic regulatory mechanism characterized by the production of endogenous cardiac glycosides that may control potentially detrimental increases in Na^+,K^+-ATPase activity during specific contexts in vivo, thereby preventing autotic tissue cell death.

Here, we report that Na^+,K^+-ATPase and the autophagy protein Beclin 1 interact in a wide range of conditions, including autophagy-inducing treatments in vitro, mice subjected to starvation, patients with anorexia nervosa and animal models of cerebral and renal ischemia. Furthermore, cardiac glycosides decrease the Na^+,K^+-ATPase/Beclin 1 interaction, the numbers of autotic cells, and the severity of ischemic injury. Moreover, endogenous cardiac glycosides block the increased Na^+,K^+-ATPase/Beclin 1 interaction and autosis during exercise, a physiological inducer of autophagy. Taken together, our results show a new, unexpected link between two pathways oppositely involved in cellular energy balance whose regulation may define cell fate in different physiological and pathological conditions.

Results

Identification of autosis regulators in a genome-wide siRNA screen.

A previous chemical screen revealed that cardiac glycosides, antagonists of Na^+,K^+-ATPase, are inhibitors of autosis (13). To further characterize autotic cell death and identify potential mediators of the pathway, we performed a genome-wide siRNA screen using a Dharmacon Human siGENOME siRNA library. Following transfection with the siRNA library, HeLa cells were then treated with the autophagy-inducing peptide Tat-Beclin 1 (26) and cell viability was assessed by measuring cellular ATP levels using the CellTiter-Glo assay. (Supplemental Figure 1A). For the top 240 hits of the primary screen (defined as those with z scores $\geq$ 3.0) (Supplemental Figure 1, B and C; Supplemental Table 1), we performed a confirmation screen using the SYTOX Green assay for cell death (Supplemental Figure 1B). Those genes whose silencing resulted in a reduction of autotic cell death of > 40% were chosen for further analysis (Supplemental Table 2). After eliminating genes that decreased Tat-Beclin 1 peptide entry into the cells, we performed a deconvolution screen using individual siRNAs. This screen identified 13 candidate regulators of autosis whose inhibition resulted in greater than 40% protection against autotic cell death. Notably, the strongest scoring hit was the α1 subunit of Na^+,K^+-ATPase (ATP1A1), confirming an essential role for the Na^+,K^+-ATPase pump in autosis (Supplemental Table 3).

Beclin 1 and Na^+,K^+-ATPase interact during autophagy- and autosis-inducing conditions.

As both a prior chemical screen (6) and our current genome-wide siRNA screen indicated that Na^+,K^+-ATPase is an essential effector of autosis, we further investigated the molecular link between Na^+,K^+-ATPase and autophagy during autotic cell death. A map of the human

autophagy network previously suggested that Beclin 1 may bind the alpha subunit of Na^+,K^+-ATPase (27). Thus, we hypothesized that the interaction between Beclin 1 and Na^+,K^+-ATPase may be regulated during different conditions where autophagy is induced, including autosis.

To investigate this hypothesis, we first used starvation or Tat-Beclin 1 peptide treatment to induce autophagy in HeLa cells in vitro. In both cases, the amount of Beclin 1 that immunoprecipitated with Na^+,K^+-ATPase increased (Figure 1A and Supplemental Figure 2A). However, this binding was reduced by treatment with the cardiac glycoside, digoxin. Furthermore, using proximity ligation assays (PLA), we observed increased Beclin 1/Na^+,K^+-ATPase interaction after starvation or Tat-Beclin 1 treatment which was reduced by digoxin (Figure 1B-C and Supplemental Figure 2B-C). This interaction occurs not only at the plasma membrane but also at different intracellular compartments such as the nuclear membrane, the endoplasmic reticulum, the mitochondria and early endosomes (Figure 1D-E). Moreover, the increase in Beclin 1/Na^+,K^+-ATPase binding after prolonged starvation was more pronounced in autotic than in apoptotic cells (Supplementary Figure 3). Importantly, prolonged nutrient starvation in mice also led to enhanced Beclin 1/Na^+,K^+-ATPase interaction in mouse hearts and livers, as demonstrated both by co-immunoprecipitation and proximity ligation assays (Figure 2, A-F). Furthermore, livers from patients with anorexia nervosa that previously exhibited autotic cells (7) also showed a markedly increased binding of Beclin 1 to the Na^+,K^+-ATPase pump (Figure 1G and H). Collectively, these results suggest that enhanced interaction between Beclin 1 and Na^+,K^+-ATPase occurs both in vitro during autophagy-inducing conditions and in vivo following extended nutrient deprivation.

Beclin 1 and Na^+,K^+-ATPase interact during ischemic injury

We next investigated whether the Beclin 1/Na^+,K^+-ATPase interaction increases in vivo during tissue ischemia. Previously, we described autotic cell death in neonatal rat brains subjected to hypoxia-ischemia (HI) injury and demonstrated that autotic death, as well as central nervous system (CNS) infarct size, were reduced by a CNS-penetrating cardiac glycoside, neriifolin (6). Using this same model of rat neonatal cerebral HI, we measured Beclin 1/Na^+,K^+-ATPase interaction by co-immunoprecipitation and proximity ligation assays. The brains of rats subjected to cerebral HI injury displayed an increase in Beclin 1/Na^+,K^+-ATPase association compared to the brains of control sham-operated animals (Figure 3, A-D) and neriifolin prevented this increase. Thus, Beclin 1/Na^+,K^+-ATPase interaction is enhanced in an established model of ischemia-induced autotic cell death (rat neonatal cerebral HI) and the interaction of these proteins is inhibited by a cardiac glycoside previously shown to exert beneficial effects in this model (6).

We then examined whether increased Beclin 1/Na^+,K^+-ATPase interaction occurred in another rodent tissue ischemia model – renal ischemia reperfusion injury (IRI) secondary to renal artery ligation. The kidneys of mice examined 48 hours after IRI displayed increased association between Beclin 1 and Na^+,K^+-ATPase (as demonstrated by co-immunoprecipitation and proximity ligation assays) compared to kidneys from control sham-operated mice (Figure 3, E-H). Moreover, this increase was blocked by the cardiac glycoside, ouabain, further confirming that digoxin-like molecules regulate the interaction between Beclin 1 and Na^+,K^+-ATPase in ischemic injury.

Ouabain decreases autotic cell death and improves outcome in renal ischemia reperfusion injury

Analogous to observations in the rat neonatal cerebral HI model (6) Figure 3, A-D), the increase in Beclin 1/Na^+,K^+-ATPase interaction in kidneys of mice subjected to IRI was associated with increased autotic death. Electron microscopic analyses of kidneys 48 hours after IRI revealed a marked increase in the number of cells that displayed the unique morphological features of autosis (including the expansion of the perinuclear space and a concave nucleus) (Figure 4A and B). This increase in autotic cell death was blocked by ouabain. Autotic cell death was observed in renal peritubular capillary regions (mainly pericytes) and not in renal tubular cells. This observation is consistent with previous studies indicating that pericyte loss during acute kidney injury is associated with permanent peritubular capillary rarefaction, tubular damage and renal fibrosis (28, 29). Notably, in parallel with reducing Beclin 1/Na^+,K^+-ATPase interaction and decreasing autotic cell death, treatment with ouabain also improved renal histopathology (Fig. 4, C-D) and enhanced renal function as measured by serum levels of BUN and creatinine after IRI (Figure 4, E-F). Moreover, while ~25% of the injured mice treated with vehicle died during the 48 hours of reperfusion, all of the mice treated with ouabain survived (data not shown). Together with our previous study (6), these results demonstrate that autosis occurs during ischemic injury, and that cardiac glycosides may be beneficial in reducing autosis and end-organ damage during tissue ischemia.

Endogenous cardiac glycosides regulate Beclin 1/Na^+,K^+-ATPase binding and autosis during exercise

Previous studies have identified the presence of endogenous cardiac glycosides in mammals (30) and have shown that their plasma concentrations increase during exercise (25). Given the

regulation of the Beclin 1/Na^+,K^+-ATPase interaction by cardiac glycoside drugs, we asked whether endogenous cardiac glycosides might prevent the increase in the Beclin 1/Na^+,K^+-ATPase interaction during exercise. Even though exercise is a well-established physiological inducer of autophagy (31, 32), it did not increase Beclin 1/Na^+,K^+-ATPase binding in hearts from mice after 80 minutes of running on a treadmill, as shown by co-immunoprecipitation and proximity ligation assays (Figure 5, A-D). However, this interaction increased when mice were treated with DigiFab, an antibody that effectively blocks endogenous digoxin-like molecules (33), before running on the treadmill (Figure 5, A-D). Moreover, the hearts from mice that were subjected to both DigiFab treatment and exercise showed an increase in detectable autotic cells (Figure 5, E and F). Notably, only non-myocytes (i.e., fibroblasts) were found to die by autosis, resembling the cell type-specific susceptibility to autosis that we observed in the kidney. Taken together, these results indicate that endogenous cardiac glycosides may regulate Beclin 1/Na^+,K^+-ATPase interaction during exercise while preventing autotic cell death.

Discussion

Our study defines an essential role of Na^+,K^+-ATPase in autotic cell death and uncovers unexpected cross-talk between Na^+,K^+-ATPase and the autophagy protein Beclin 1 during physiological and pathophysiological stress. Specifically, we show that Na^+,K^+-ATPase and Beclin 1 interact in cells during nutrient starvation, in rodent tissues during starvation and ischemic injury, and in livers of patients with severe anorexia nervosa. Cardiac glycosides, antagonists of Na^+,K^+-ATPase, inhibit this interaction during neonatal rat cerebral hypoxia-ischemia injury and mouse renal ischemia in parallel with improving clinical outcomes and decreasing autotic cell death. Moreover, blockade of endogenous cardiac glycosides during exercise increases Na^+,K^+-ATPase/Beclin 1 interaction and autotic cell death in the heart. This cross-talk between the cell's major consumer of ATP (Na^+,K^+-ATPase) and a key generator of ATP during nutrient stress (autophagy) represents a newly described nexus for the regulation of cell survival.

Further studies are required to definitively determine whether, and if so how, the Na^+,K^+-ATPase/Beclin 1 interaction causes autotic cell death. In theory, the interaction could (1) alter Na^+,K^+-ATPase ion exchange or Na^+,K^+-ATPase ion exchange-independent effects on cellular signaling; (2) alter functions of Beclin 1 in autophagy or related-membrane trafficking events; and/or (3) exert effects on the cell not directly related to known functions of Na^+,K^+-ATPase or Beclin 1. The robust induction of autophagy during tissue starvation (32, 34) suggests that enhanced Na^+,K^+-ATPase/Beclin 1 interaction does not inhibit the function of Beclin 1 in autophagy. Of note, the unique morphology of autosis involves endoplasmic reticulum (ER) and focal perinuclear space expansion, phenotypes that have been observed in cells with mutations in genes that affect ER membrane properties, including transport or channel conductance (35). It is

thus relevant to note that we observed Na^+,K^+-ATPase/Beclin 1 interaction not only at the plasma membrane, but also (and more frequently) on intracellular membranes such as the ER and perinuclear membrane as well as mitochondria and endosomes. Although best known for its plasma membrane localization, Na^+,K^+-ATPase has also been reported to localize to the perinuclear membrane, ER, mitochondria and endosomes (36-38) with some evidence for nuclear envelope Na^+,K^+-ATPase-dependent regulation of local Na^+; K^+ gradients and calcium signaling (36). Thus, delineation of the effects of Na^+,K^+-ATPase and Beclin 1 interaction on ion, osmolyte and fluid homeostasis across intracellular membranes may help elucidate the basis for the distinct morphological features of autosis as well as potential mechanisms whereby the interactions between these proteins could lead to cell death.

In addition to Na^+,K^+-ATPase, our genome-wide siRNA screen identified other potential mediators of autosis (Supplemental Tables 1-3). Related to our hypothesis that autosis may involve a dysregulation of ion transport, other confirmed hits included genes encoding the intermediate conductance calcium-activated potassium channel protein 4 (KCNN4) and the potassium voltage-gated channel subfamily KQT member 2 (KCNQ2). In addition, a key feature that distinguishes autosis from other forms of cell death is the increased cellular substrate adherence (6); accordingly, the identification of genes involved in cell-to-matrix adhesion such as adhesion G protein-coupled receptor F1 (ADGRF1) and thrombospondin 3 (THBS3) may indicate a requirement for increased cell-to-matrix adhesion in the autotic death pathway. Further studies are needed to investigate the role of these, and additional genes found in our genome-wide screen, in autosis.

We discovered an important role for cardiac glycoside drugs (e.g. digoxin, neriifolin, and ouabain) and endogenous cardiac glycosides in regulating the interaction between Na^+,K^+-

ATPase and Beclin 1 during starvation, cerebral hypoxia-ischemia injury, renal ischemia reperfusion injury, and exercise. Exogenous cardiac glycosides decrease the interaction and prevent autotic death during cellular starvation, rat cerebral hypoxia-ischemia injury, and renal ischemia reperfusion (the present study and (6)), whereas blockade of endogenous cardiac glycosides with DigiFab increases Na^+,K^+-ATPase/Beclin 1 interaction and autosis during exercise in cardiac tissue. Previously, we showed that neriifolin improves clinical outcomes in rats with neonatal cerebral hypoxia-ischemia injury (6) and in the current study, we found that ouabain improves clinical outcomes in mice with renal ischemia reperfusion injury. Thus, even though it is unknown whether Beclin 1/Na^+,K^+-ATPase interaction is a driving event in autosis, our findings raise the possibility that cardiac glycosides may be clinically useful in settings of tissue ischemia and autotic cell death. Moreover, we speculate that endogenous cardiac glycosides may represent an adaptive mechanism that regulates Na^+,K^+-ATPase activity, preventing its association with the autophagy machinery and allowing autophagy to be protective rather than pathological during stress.

An open question is how cardiac glycosides disrupt the interaction between Na^+,K^+-ATPase and Beclin 1. Cardiac glycosides bind to the extracellular domain of the α subunit of Na^+,K^+-ATPase and thereby inhibit Na^+/K^+ exchange as well as regulate diverse cellular signal transduction pathways (20). It is possible cardiac glycoside binding could trigger a conformational change in Na^+,K^+-ATPase that directly prevents its interaction with Beclin 1 on the cytoplasmic side of either the plasma membrane or intracellular membranes. It is also possible that one of the signaling cascades triggered by cardiac glycosides, such as activation of epidermal growth factor receptor tyrosine kinase (39) that phosphorylates Beclin 1 (40), indirectly alters the ability of Beclin 1 to interact with Na^+,K^+-ATPase. Interestingly, one

previous study reported that EGFR functions as a switch between cell survival and cell death induced by autophagy in hypoxic cancer cells (8). Our detection of a Na^+,K^+-ATPase/Beclin 1 interaction at endosomes may indicate that its regulation occurs during the trafficking of Na^+,K^+-ATPase. However, the predominant localization of the interaction at intracellular membranes (e.g. mitochondria, ER/perinuclear membrane) suggests potential alternative mechanisms of regulation. Although cardiac glycosides are reported to enter cells through either passive diffusion (for those compounds such as digoxin that are hydrophobic) or uptake by drug transporters (41, 42), it is unclear how they would gain access to the extracellular domain of Na^+,K^+-ATPase (which would be on the luminal side of intracellular membranous compartments). Therefore, it seems more likely that interactions between Na^+,K^+-ATPase/Beclin 1 at the mitochondria and ER/perinuclear membrane are regulated indirectly via cardiac glycoside effects on ionic concentrations or signal transduction pathways. To unravel the precise mode of regulation of Na^+,K^+-ATPase/Beclin 1 interaction by cardiac glycosides, as well as its significance in autotic cell death, an atomic understanding of the interaction will be essential.

Methods

Cell culture. HeLa cells were obtained from American Type Culture Collection and cultured in DMEM supplemented with 10% (vol/vol) FBS, 1% L-Glutamine and 1% penicillin/streptomycin. For starvation experiments, cells were cultured in Hanks' Balanced Salt Solution (HBSS) (Sigma, H4641) for the indicated time.

Chemical reagents and antibodies. Digoxin was purchased from Sigma (D6003). The following antibodies were used for immunoblot analyses: anti-Na^+,K^+-ATPase α2 subunit (used in analyses of mouse hearts, livers and kidneys, Proteintech, 18836-1-AP, 1:100 dilution), anti-Na^+,K^+-ATPase α3 subunit (used in analyses of rat brains, Abcam, ab182571 and ab2826, 1:1000 dilution), anti-Beclin 1 (Santa Cruz Biotechnology, sc-11427: 1:250 dilution) and anti-Actin (Santa Cruz Biotechnology, sc-47778; 1:5,000 dilution; and ThermoFisher Scientific (Invitrogen), MA511869, 1:2000 dilution). The following antibodies were used for immunofluorescence analyses: anti-Na^+,K^+-ATPase α1 subunit (used in analyses of human liver samples, Santa Cruz Biotechnology, sc-21712; 1:50 dilution), anti-Na^+,K^+-ATPase α2 subunit (used in analyses of mouse hearts, livers and kidneys, Proteintech, 18836-1-AP, 1:100 dilution), anti-Na^+,K^+-ATPase α3 subunit (used in analyses of rat brains, Abcam, ab182571; 1:1000 dilution), anti-Beclin 1 (Santa Cruz Biotechnology, sc-11427 and sc-10086; 1:100 dilution), anti-EEA1 (Santa Cruz Biotechnology, sc-6415, 1:50 dilution), anti-HSP60 (Santa Cruz Biotechnology, sc-1052, 1:50 dilution), anti-PDI (Santa Cruz Biotechnology, sc-30932, 1:50 dilution) and anti-Lamin A/C (Santa Cruz Biotechnology, sc-6215, 1:50 dilution). Anti-Wheat German Agglutinin (WGA) conjugated with Alexa Fluor 488 (ThermoFisher Scientific, W11261, 1:200) was used to stain the plasma membrane according to manufacturer's instructions.

Genome-wide siRNA screen. For the primary screen, 800 HeLa cells per well were transfected with 2 pmol human Dharmacon Human siGENOME siRNA Library (Horizon Discovery, Inc.) using 0.1 µl Lipofectamine RNAiMAX (Thermo Scientific, #13778150) in 96-well plates (Greiner Bio-one, 655083). After 48 hours of transfection, cells were treated with 12.5 µM Tat-Beclin 1 peptide (YGRKKRRQRRRGGTNVFNATFEIWHDGEFGT) in 100 µl acidified Opti-MEM (pH 6.8) for 4 hours and then lysed in 40 µl CellTiter-Glo solution (Promega, G8462). Cellular ATP levels were measured by an EnVision multimode plate reader (Perkin-Elmer, Inc.). Wells in the first column and the last column of each 96-well plate were transfected with NC siRNA (Thermo Scientific, D-001210-02-20) and *ATP1A1* siRNA (Invitrogen, 4390824, CUCGCUCACUGGUGAAUCA) respectively. Each siRNA pool (4 siRNAs) was screened in triplicate. For the primary screen, we first fitted a liner model to compare the differences between the siRNAs triplicates with negative controls on the same plate to estimate the Z-score and folder change. Second, raw data from Envision Reader were analyzed with Genedata Screener® 11 software suite (Genedata AG, Basel, Switzerland). First, .txt or .csv data files were loaded into Assay Analyzer module of Genedata software, and normalized by the test population (the transfecting siRNA library) in each plate, using the following equation (43):

$$Normalized\ Values = \frac{Raw\ Values - Median\ Of\ All\ Samples}{Median\ Of\ All\ Samples} * 100$$

An average Z'-factor of 0.54 was achieved in the entire screen. Normalized well values were then corrected using a group of reference plates (typically 3 plates with sequence scrambled siRNA, placed at the first, middle and last position of a 30-plate run). A correction factor for each well was calculated using a proprietary pattern detection algorithm in the Assay Analyzer software (See GeneData user documentation and (44)). The corrected normalized activity values from replicates for each siRNA in each run were then condensed to a single value (condensed activity) using the "Robust Condensing"

method in Genedata Screener®. The condensed activity is the most representative single value of the triplicates. In general, the triplicates were pre-condensed into a pair of values as follows:

$$Values(X, Y) = (Median\ of\ Triplicates\ m) \pm Dispersion$$

where Dispersion = Median (|X1-m|, |X2-m|, |X3-m|). The less X and Y differ (|X-Y|), the better the data quality. For data points where |X-Y| <= 30%, the condensed activity is equal to the median of the triplicate measurements. Otherwise, a condensing function Max(X, Y) was used to estimate the condensed activity. Calculation of condensed activity values from triplicated measurements was implemented with a Pipeline Pilot protocol (BIOVIA, San Diego, CA). A robust Z-score was calculated from the corrected normalized activity for each siRNA by using the following formula (44):

$$Robust\ Zscore = \frac{(Corrected\ Activity - Median\ of\ neutral\ controls)}{Robust\ SD\ of\ neutral\ controls}$$

The Z-scores estimated by linear model and robust z-score were averaged to get the final z-score. Primary hits were selected if the final z-score was equal or greater than 3.0. For the confirmation screen, 1,000 HeLa cells were transfected with 2 pmol the human Dharmacon siGENOME siRNA Library using 0.1 µl Lipofectamine RNAiMAX (Thermo Scientific, #13778150) in a 96-well plate (Greiner Bio-one, 655090). Forty-eight hours after transfection, cells were treated with 18 µM Tat-Beclin 1 peptide in 100 µl acidified Opti-MEM (pH 6.8) for 4 hours and then 100 nM SYTOX Green (Invitrogen, S7020) and 1 µg/ml Hoechst 33342 was added for one additional hour. Cells were then imaged using a BD Pathways 855 automated microscope. Cells in the first column and the last column of each 96-well plate were transfected with NC siRNA (Thermo Scientific, D-001210-02-20) and *ATP1A1* siRNA (Invitrogen, 4390824, CUCGCUCACUGGUGAAUCA) respectively. Each siRNA was screened in triplicate. Autotic cell death was counted as the percentage of SYTOX Green-positive cells. The protection of each

siRNA was calculated as follows ("A" means the observed autotic cell death as a percentage of SYTOX green-positive cells from triplicate plates)

$$Protection(siRNA) = \frac{A(NC) - A(siRNA)}{A(NC) - A(ATP1A1)} \times 100\%$$

For the deconvolution screen, 1,000 HeLa cells were transfected with 2 pmol of each siRNA from the SMART pool for each gene (4 siRNAs per gene) in the Dharmacon Human siGENOME siRNA library or the Invitrogen Ambion Silencer Select siRNA using 0.1 μl Lipofectamine RNAiMAX (Thermo Scientific, #13778150) in 96-well plates (Greiner Bio-one, 655090). Forty-eight hours after transfection, cells were treated with 18 μM Tat-Beclin 1 in 100 μl acidified Opti-MEM (pH6.8) for 4 hours and then 100 nM SYTOX Green and 1 μg/ml Hoechst 33342 was added for one additional hour. Cells were then imaged using a Bio-Tek Cytation 3 Cell Imaging Multi-Mode Reader. Cells in the first column and the last column of each 96-well plate were transfected with NC siRNA (Thermo Scientific, D-001210-02-20) and *ATP1A1* siRNA (Invitrogen, 4390824, CUCGCUCACUGGUGAAUCA) respectively. Each siRNA was screened in triplicate.

Peptide entry assay. N-terminal biotinylated Tat-Beclin 1 peptide (>95% purity as determined by RP-HPLC) was synthesized as described (26). For the peptide entry assay, siRNA transfected cells were treated with 20 μM biotinylated Tat-Beclin 1 for 30 minutes, fixed with 4% paraformaldehyde at room temperature for 10 minutes, and permeabilized with Triton X-100 solution (0.5% Triton X-100, 20 mM Hepes pH7.4, 50 mM NaCl, 3 mM $MgCl_2$, 300 mM sucrose) for 5 minutes on ice. After staining with Alexa Fluor 488-conjugated streptavidin for 1 hour, more than 400 cells per siRNA treatment were imaged using a Perkin Elmer Ultraview spinning disk confocal microscope. Cells showing the typical intracellular staining pattern of Alexa Fluor 488 signal were counted as biotin-positive cells.

Renal ischemia-reperfusion injury (IRI) model. Eight to twelve week-old wild-type mice (C57Bl/6J, Jackson Laboratories) underwent bilateral ischemia for 45 minutes followed by 48 hours reperfusion. Laparotomy was conducted for sham treatment in control animals following our previously published protocol (45). Vehicle (0.5% ethanol/PBS) or ouabain (0.25 mg/kg diluted in 0.5% ethanol/PBS) (Sigma, O3125) was injected intraperitoneally 30 minutes prior to surgery. After 48 hours reperfusion, mice were euthanized under anesthesia and blood and kidneys were harvested. The kidney samples were either fixed in 4% paraformaldehyde for paraffin-embedded sections used for histopathological analyses or fixed in Karnovsky's fixative (2.5% glutaraldehyde, 4% paraformaldehyde, 0.1 M cacodylate buffer, 8 mM CaCl2, pH 7.4) for ultrastructural analysis. The severity of kidney damage was semi-quantified with a kidney histological score in a blinded manner as adapted from previous publications (45, 46). Briefly, the kidney injury was scored in hematoxylin and eosin stained kidney sections as percentage of damaged tubules: 0, no damage; 1, damage in less than 25% of the field; 2, damage in 25–50% of the field, 3, damage in 50–75% of the field, 4, damage in more 75% of the field. Plasma BUN was analyzed using a Vitros Chemistry Analyzer (Ortho-Clinical Diagnosis, Rochester, NY). Plasma creatinine was measured using a P/ACE MDQ Capillary Electrophoresis System and photodiode detector (Beckman-Coulter, Fullerton, CA), as previously described (47).

In vivo starvation studies. Eight week-old wild-type mice (C57Bl/6J, Jackson Laboratories) were starved overnight and re-fed for 3 h before sample collection (control group) or 48 hours of starvation (starved group) to minimize variability due to differences in food intake.

Mouse exercise studies. Eight-to-twelve week-old wild-type mice (C57Bl/6J, Jackson Laboratories) were acclimated to a 10º uphill Exer 3/6 open treadmill (Columbus Instruments) for 2 days. On day 1, mice ran for 5 minutes at 8 m/minute and on day 2 mice ran for 5 minutes at 8 m/minute followed by another 5 minutes at 10 m/minute. On day 4 mice were treated either with vehicle or DigiFab (10 µg/kg) 30 minutes before being subjected to a single bout of running starting at the speed of 10 m/minute. Forty minutes later, the treadmill speed was increased at a rate of 1 m/minute every 10 minutes for a total of 30 minutes, and then increased at the rate of 1 m/minute every 5 minute until they ran for a total of 80 minutes (for co-immunoprecipitations or proximity ligation assays, with sample collection immediately after exercise) or until they were exhausted (for electron microscopy analysis, with sample collection 6 hours later). Exhaustion was defined as the point at which mice spent more than 5 seconds on the electric shocker without attempting to resume running. Mice were euthanized and hearts were then harvested. The samples were either frozen for western blot analyses, fixed in 4% paraformaldehyde (embedded thereafter in 30% sucrose to prepare cryosections) for proximity ligation assays or fixed in Karnovsky's fixative (2.5% glutaraldehyde, 4% paraformaldehyde, 0.1 M cacodylate buffer, 8 mM CaCl2, pH 7.4) for electron microscopy analysis.

Rat model of neonatal cerebral hypoxia-ischemia (HI). Seven-day-old male rats (Sprague Dawley, from Janvier, France) underwent hypoxia/ischemia (HI) according to the Rice-Vannucci model (48) as described previously (49). Briefly, under isoflurane (3%) anaesthesia, the right common carotid artery was isolated, double-ligated and cut. One hour after carotid occlusion, neriifolin (0.22 mg/kg diluted in 0.5% ethanol/PBS) (Sigma, S961825) or vehicle (0.5% ethanol/PBS) was injected intraperitoneally. After a total of 2 hours of recovery with the dam, the rat pups were exposed to 2 hours of systemic

hypoxia at 8% of oxygen in a chamber maintained around 35.5 °C. Sham-operated animals (same anaesthesia and surgery without cutting the artery) were used as controls. Hippocampal samples were microdissected and collected 6 hours after hypoxia.

Immunoprecipitation. HeLa cells were collected and lysed in lysis buffer (20 mM Tris-HCl, 100 mM KCl, 4 mM $MgCl_2$, 10% glycerol, 1% Triton X-100, protease inhibitor mixture (Roche Applied Sciences), and halt phosphatase inhibitor mixture (Thermo Scientific), pH 7.4). Anti-human Na^+,K^+-ATPase α1 subunit antibody (Santa Cruz Biotechnology, sc-21712; 1:100 dilution), or control IgG (Santa Cruz, sc-2025) was then added to the lysate, and incubated at 4°C for 1 hour. Protein G PLUS-Agarose (Santa Cruz, sc-2002) was then added (1:25 dilution) and samples were incubated at 4°C overnight. The beads were pelleted, washed, boiled with 2x Laemmli buffer and the supernatant was resolved on SDS-PAGE. For immunoprecipitation assays in mouse tissues, protein samples were obtain using a different lysis buffer, containing 250 mM HEPES, 250 Mm KCl, 250 mM NaF, 25 mM $Na_4P_2O_7$, 25 mM beta-glycerophosphate, 5 mM EDTA, 5 mM EGTA, 200 mM vanadate, 500 mM DTT and protease inhibitor mixture (Roche Applied Sciences). Samples were then incubated overnight with anti-mouse Beclin 1 antibody (Santa Cruz Biotechnology, sc-48341, 1:100) and Protein-A Sepharose beads (Sigma, P-3391). The beads were pelleted, washed, transferred to a new tube, boiled with 2x Laemmli buffer and the supernatant was resolved on SDS-PAGE. For immunoprecipitation assays in rat brains, whole hippocampal tissues were collected in lysis buffer (20 mM HEPES, pH 7.4, 10 mM NaCl, 3 mM MgCl2, 2.5 mM EGTA, 0.1 mM dithiothreitol, 50 mM NaF, 1 mM Na3VO4, 1% Triton X-100 and a protease inhibitor cocktail (Sigma; 11873580001)), homogenized on ice and rapidly sonicated. After protein concentration determination using a Bradford assay, 500 µg of proteins were incubated in 300 µl of immunoprecipitation (IP) buffer (25mM Tris, 150mM NaCl, 1% NP40, 1mM Na3VO4,

20mM NaF and a protease inhibitor cocktail (Sigma)) with 1-1.5 µg of antibody (anti-Na^+,K^+-ATPase α3 subunit rabbit monoclonal (ab182571) from Abcam or anti-Beclin 1 (sc-11427) rabbit polyclonal or (sc-48341) mouse monoclonal from Santa Cruz Biotechnology) overnight at 4°C. Control IP was performed with an isotype control antibody (3900S) from Cell Signaling or with an anti-GFP (AB3080) from Merk/Millipore. After washing three times in IP buffer, 30-40 µl of Dynabeads™ Protein G (10004D) from ThermoFisher Scientific (Invitrogen) were added to antibody/antigen complex and incubated 90 minutes at 4°C. Dynabeads were then washed 3 times in IP buffer, resuspended in 100 µl of IP buffer and transferred to a new tube. Antibody/antigen complex was eluted by heating at 95°C for 10 minutes in 40 µl of 2x SDS loading buffer (125mM TRIS pH 6.8, 4% SDS, 12.5% glycerol, 4% β-mercaptoethanol). The eluted samples were separated by SDS-PAGE, transferred on nitrocellulose membrane and analyzed by immunoblotting as previously described (50) except that IRDye 680RD Detection Reagent (926-68100) from Li-COR or Fluorescent TrueBlot IgG DyLight secondary antibodies (18-4516-32, 18-4417-32) from Rockland Immunochemicals were used. Optical densities of bands were quantified using Odyssey v1.2 software (LI-COR).

Proximity ligation assay. The proximity ligation assay (PLA) was performed according to the manufacturer's instructions (Sigma, DUO92008). Briefly, cells were fixed with 3% paraformaldehyde for 10 minutes at room temperature and cold methanol for 20 minutes at 4°C, and then blocked with 0.05% saponin, 1% BSA in PBS for 1 hour at room temperature. After incubation with primary antibodies overnight, cells were washed with 0.05% saponin, 1% BSA in PBS twice for 10 minutes. Cells were then incubated with Duolink In Situ PLA Probe anti-rabbit PLUS and Duolink In Situ PLA Probe anti-mouse MINUS (1:5 dilution) for 60 minutes at 37°C and then washed with Buffer A twice for 10 minutes. Ligase was added at 1:40 dilution and incubated for 30 minutes at 37°C. After washing

with Buffer A twice for 5 minutes, PLA signal was amplified by Polymerase (1:80) for 100 minutes at 37°C. Cells were then washed with 1x Buffer B twice for 20 minutes and then 0.01x Buffer B for 1 minute and mounted in Duolink In Situ Mounting Medium with DAPI for 15 minutes. For tissues, frozen sections were incubated in LAB solution (Polysciences, #24310-500) at 65°C for 5 minutes and then washed with PBS once. The samples were then incubated in 15 ml/L hydrogen peroxide in PBS for 15 minutes at room temperature and washed with PBS once. The standard PLA protocol was then performed starting from the blocking step.

Microscopy. Immunofluorescent images were captured using either a Zeiss Axio Imager Z2 microscope or a LSM 780 Meta confocal microscope (Carl Zeiss). Electron microscopy images were captured using a JEOL 1200 EX II Electron Microscope (UT Southwestern Electron Microscopy Core). SYTOX Green assay was analyzed using a BD Pathways 855 automated microscope.

Statistics. Experimental data were analyzed using the GraphPad Prism 8 software. *P* values were calculated using two-tailed Student's *t* test and one or two-way ANOVA (for multiple groups analyses) followed by Tukey post hoc test. Standard error of the mean (SEM) was used when the individual data points represented mean values for a population of cells. Standard deviation (SD) was used when data points represented the value of an individual sample.

Study approval. All human studies were conducted according to Declaration of Helsinki principles. The biopsies of human livers for research purposes and their analyses have been approved by the appropriate Institutional Review Board (Inserm Institutional Review Board, 00003888), and all participants gave written informed consent. All experiments involving mice were conducted following

the Guide for the Care and Use of Laboratory Animals by the National Institutes of Health and were approved by the Institutional Animal Care and Use Committee at UT Southwestern Medical Center. All experiments involving rat perinatal cerebral hypoxia-ischemia were performed in accordance with the Swiss Laws for the protection of animals and were approved by the Vaud Cantonal Veterinary Office.

Author contributions

A.F.F., Y.L., V.G., J.P., M.C.H. and B.L. designed the study. A.F.F., Y.L., V.G. and Z.Z. performed biochemical and fluorescence microscopic analyses. A.F.F and Y.L. performed electron microscopy analysis. V.G. and M.S. performed animal surgeries. M.C.H. performed histological analyses. A.Z., B.A.P. and G.X. performed bioinformatics analyses. M.T., V.P. and P.-E.R assisted with studies of livers from patients. A.F.F., Y.L., V.G., J.N., J.S., P.-E.R., J.P., M.C.H. and B.L. discussed and analyzed data. A.F.F. and B.L. wrote the manuscript.

Acknowledgements

The authors thank L. Nguyen for technical assistance and H. Smith for assistance with manuscript preparation. This work was supported by NIH grants RO1 CA109618 (B.L.), U19 AI109725 (B.L), U19 AI142784 (B.L.), RO1 DK091392 (M.C.H.), RO1 DK092461 (M.C.H.), and 5P30 CA124543 (A.Z. and B.A.P.), RO1 HL138720 (J.S.); Cancer Prevention Research Institute of Texas grant RP120718 (B.L.); a Fondation Leducq grant 15CBD04 (J.S., B.L.); the Pak Foundation for Endowed Professors Collaborative Research Support (M.C.H); the “Institut National de la Santé et de la Recherche Médicale” (ATIP AVENIR) (P.-E.R.); the “Agence Nationale pour la Recherche” (ANR-14-CE12-0011, ANR-14-CE35-0022, ANR-18-CE14-0006-01) (P.-E.R.); the Swiss National Foundation (310030, 163064, 310030, 182332) (J.P.); and a Fondation Motrice grant (J.P.).

References:

1. Kroemer G, Marino G, and Levine B. Autophagy and the integrated stress response. *Mol Cell.* 2010;40(2):280-93.

2. Feng Y, He D, Yao Z, and Klionsky DJ. The machinery of macroautophagy. *Cell Res.* 2014;24(1):24-41.

3. Singh R, and Cuervo AM. Autophagy in the cellular energetic balance. *Cell Metab.* 2011;13(5):495-504.

4. Bialik S, Dasari SK, and Kimchi A. Autophagy-dependent cell death - where, how and why a cell eats itself to death. *J Cell Sci.* 2018;131(18).

5. Galluzzi L, Vitale I, Aaronson SA, Abrams JM, Adam D, Agostinis P, et al. Molecular mechanisms of cell death: recommendations of the Nomenclature Committee on Cell Death 2018. *Cell Death Differ.* 2018;25(3):486-541.

6. Liu Y, Shoji-Kawata S, Sumpter RM, Jr., Wei Y, Ginet V, Zhang L, et al. Autosis is a Na+,K+-ATPase-regulated form of cell death triggered by autophagy-inducing peptides, starvation, and hypoxia-ischemia. *Proc Natl Acad Sci U S A.* 2013;110(51):20364-71.

7. Kheloufi M, Boulanger CM, Codogno P, and Rautou PE. Autosis occurs in the liver of patients with severe anorexia nervosa. *Hepatology.* 2015;62(2):657-8.

8. Chen Y, Henson ES, Xiao W, Huang D, McMillan-Ward EM, Israels SJ, et al. Tyrosine kinase receptor EGFR regulates the switch in cancer cells between cell survival and cell death induced by autophagy in hypoxia. *Autophagy.* 2016;12(6):1029-46.

9. Zhang G, Luk BT, Hamidy M, Zhang L, and Spector SA. Induction of a Na(+)/K(+)-ATPase-dependent form of autophagy triggers preferential cell death of human immunodeficiency virus type-1-infected macrophages. *Autophagy.* 2018:1-17.

10. Ginet V, Pittet MP, Rummel C, Osterheld MC, Meuli R, Clarke PG, et al. Dying neurons in thalamus of asphyxiated term newborns and rats are autophagic. *Ann Neurol.* 2014;76(5):695-711.

11. Ravikumar B, Sarkar S, Davies JE, Futter M, Garcia-Arencibia M, Green-Thompson ZW, et al. Regulation of mammalian autophagy in physiology and pathophysiology. *Physiol Rev.* 2010;90(4):1383-435.

12. Wang P, Shao BZ, Deng Z, Chen S, Yue Z, and Miao CY. Autophagy in ischemic stroke. *Prog Neurobiol.* 2018;163-164:98-117.

13. Kaushal GP, and Shah SV. Autophagy in acute kidney injury. *Kidney Int.* 2016;89(4):779-91.

14. Rautou PE, Mansouri A, Lebrec D, Durand F, Valla D, and Moreau R. Autophagy in liver diseases. *J Hepatol.* 2010;53(6):1123-34.

15. Matsui Y, Kyoi S, Takagi H, Hsu CP, Hariharan N, Ago T, et al. Molecular mechanisms and physiological significance of autophagy during myocardial ischemia and reperfusion. *Autophagy.* 2008;4(4):409-15.

16. Sheng R, and Qin ZH. The divergent roles of autophagy in ischemia and preconditioning. *Acta Pharmacol Sin.* 2015;36(4):411-20.

17. Descloux C, Ginet V, Clarke PG, Puyal J, and Truttmann AC. Neuronal death after perinatal cerebral hypoxia-ischemia: Focus on autophagy-mediated cell death. *Int J Dev Neurosci.* 2015;45:75-85.

18. Decuypere JP, Ceulemans LJ, Agostinis P, Monbaliu D, Naesens M, Pirenne J, et al. Autophagy and the kidney: Implications for ischemia-reperfusion injury and therapy. *Am J Kidney Dis.* 2015;66(4):699-709.

19. Nah J, Fernandez AF, Kitsis RN, Levine B, and Sadoshima J. Does autophagy mediate cardiac myocyte death during stress? *Circ Res.* 2016;119(8):893-5.

20. Diederich M, Muller F, and Cerella C. Cardiac glycosides: From molecular targets to immunogenic cell death. *Biochem Pharmacol.* 2017;125:1-11.

21. Clausen MV, Hilbers F, and Poulsen H. The structure and function of the Na,K-ATPase isoforms in health and disease. *Front Physiol.* 2017;8:371.

22. Vedovato N, and Gadsby DC. Route, mechanism, and implications of proton import during Na+/K+ exchange by native Na+/K+-ATPase pumps. *J Gen Physiol.* 2014;143(4):449-64.

23. Cui X, and Xie Z. Protein interaction and Na/K-ATPase-mediated signal transduction. *Molecules.* 2017;22(6).

24. Clausen T. Na+-K+ pump regulation and skeletal muscle contractility. *Physiol Rev.* 2003;83(4):1269-324.

25. Schoner W. Endogenous cardiac glycosides, a new class of steroid hormones. *Eur J Biochem.* 2002;269(10):2440-8.

26. Shoji-Kawata S, Sumpter R, Leveno M, Campbell GR, Zou Z, Kinch L, et al. Identification of a candidate therapeutic autophagy-inducing peptide. *Nature.* 2013;494(7436):201-6.

27. Behrends C, Sowa ME, Gygi SP, and Harper JW. Network organization of the human autophagy system. *Nature.* 2010;466(7302):68-76.

28. Zeisberg M, and Kalluri R. Physiology of the renal interstitium. *Clin J Am Soc Nephrol.* 2015;10(10):1831-40.

29. Kramann R, Wongboonsin J, Chang-Panesso M, Machado FG, and Humphreys BD. Gli1(+) Pericyte loss induces capillary rarefaction and proximal tubular injury. *J Am Soc Nephrol.* 2017;28(3):776-84.

30. Buckalew VM. Endogenous digitalis-like factors: an overview of the history. *Front Endocrinol (Lausanne).* 2015;6:49.

31. He C, Sumpter R, Jr., and Levine B. Exercise induces autophagy in peripheral tissues and in the brain. *Autophagy.* 2012;8(10):1548-51.

32. He C, Bassik MC, Moresi V, Sun K, Wei Y, Zou Z, et al. Exercise-induced BCL2-regulated autophagy is required for muscle glucose homeostasis. *Nature.* 2012;481(7382):511-5.

33. McMillin GA, Owen WE, Lambert TL, De BK, Frank EL, Bach PR, et al. Comparable effects of DIGIBIND and DigiFab in thirteen digoxin immunoassays. *Clin Chem.* 2002;48(9):1580-4.

34. Mizushima N, Yamamoto A, Matsui M, Yoshimori T, and Ohsumi Y. In vivo analysis of autophagy in response to nutrient starvation using transgenic mice expressing a fluorescent autophagosome marker. *Mol Biol Cell.* 2004;15(3):1101-11.

35. Zwerger M, Kolb T, Richter K, Karakesisoglou I, and Herrmann H. Induction of a massive endoplasmic reticulum and perinuclear space expansion by expression of lamin B receptor mutants and the related sterol reductases TM7SF2 and DHCR7. *Mol Biol Cell.* 2010;21(2):354-68.

36. Garner MH. Na,K-ATPase in the nuclear envelope regulates Na+: K+ gradients in hepatocyte nuclei. *J Membr Biol.* 2002;187(2):97-115.

37. Casciola-Rosen LA, and Hubbard AL. Lumenal labeling of rat hepatocyte early endosomes. Presence of multiple membrane receptors and the Na+,K(+)-ATPase. *J Biol Chem.* 1992;267(12):8213-21.

38. Chang CS, Kirk RG, and Lee P. Presence of immunoreactive alpha 3 subunit isoform of Na,K-ATPase in mitochondria of kidney. *Kidney Int.* 1998;54(2):457-63.

39. Haas M, Askari A, and Xie Z. Involvement of Src and epidermal growth factor receptor in the signal-transducing function of Na+/K+-ATPase. *J Biol Chem.* 2000;275(36):27832-7.

40. Wei Y, Zou Z, Becker N, Anderson M, Sumpter R, Xiao G, et al. EGFR-mediated Beclin 1 phosphorylation in autophagy suppression, tumor progression, and tumor chemoresistance. *Cell.* 2013;154(6):1269-84.

41. Nunez-Duran H, and Fernandez P. Evidence for an intracellular site of action in the heart for two hydrophobic cardiac steroids. *Life Sci.* 2004;74(11):1337-44.

42. Mikkaichi T, Suzuki T, Onogawa T, Tanemoto M, Mizutamari H, Okada M, et al. Isolation and characterization of a digoxin transporter and its rat homologue expressed in the kidney. *Proc Natl Acad Sci U S A.* 2004;101(10):3569-74.

43. Zhang JH, Chung TD, and Oldenburg KR. A simple statistical parameter for use in evaluation and validation of high throughput screening assays. *J Biomol Screen.* 1999;4(2):67-73.

44. Wu Z, Liu D, and Sui Y. Quantitative assessment of hit detection and confirmation in single and duplicate high-throughput screenings. *J Biomol Screen.* 2008;13(2):159-67.

45. Bian A, Shi M, Flores B, Gillings N, Li P, Yan SX, et al. Downregulation of autophagy is associated with severe ischemia-reperfusion-induced acute kidney injury in overexpressing C-reactive protein mice. *PLoS One.* 2017;12(9):e0181848.

46. Kaushal GP. Autophagy protects proximal tubular cells from injury and apoptosis. *Kidney Int.* 2012;82(12):1250-3.

47. Shi M, McMillan KL, Wu J, Gillings N, Flores B, Moe OW, et al. Cisplatin nephrotoxicity as a model of chronic kidney disease. *Lab Invest.* 2018;98(8):1105-21.

48. Vannucci RC, and Vannucci SJ. Perinatal hypoxic-ischemic brain damage: evolution of an animal model. *Dev Neurosci.* 2005;27(2-4):81-6.

49. Ginet V, Puyal J, Clarke PG, and Truttmann AC. Enhancement of autophagic flux after neonatal cerebral hypoxia-ischemia and its region-specific relationship to apoptotic mechanisms. *Am J Pathol.* 2009;175(5):1962-74.

50. Ginet V, Spiehlmann A, Rummel C, Rudinskiy N, Grishchuk Y, Luthi-Carter R, et al. Involvement of autophagy in hypoxic-excitotoxic neuronal death. *Autophagy.* 2014;10(5):846-60.

Figure Legends

Figure 1. Beclin 1 and Na^+,K^+-ATPase interact in cultured cells during starvation. (A) Co-immunoprecipitation of Beclin 1 with the α-subunit of Na^+,K^+-ATPase in HeLa cells after 3 hours of growth in normal media (-) or HBSS starvation media (+) treated with either vehicle or 10 μM digoxin. The same lysate from cells grown in normal media without digoxin (lane 1) was used as a control for IgG immunoprecipitation. Similar results were observed in three independent experiments. (B, C) Representative images (B) and quantitation (C) of proximity ligase assay (PLA) of Beclin 1 and Na^+,K^+-ATPase in the indicated conditions. In (C), bars represent mean values ± SEM from three independent experiments (value for each experiment represent mean value of at least 100 cells per condition). (D) Representative images of proximity ligation assays (PLA) of Beclin 1 and Na^+,K^+-ATPase co-stained with markers of plasma membrane (wheat germ agglutinin, WGA), endosomes (EEA1), mitochondria (HSP60), endoplasmic reticulum (PDI) and nuclear membrane (LAMIN A/C) in HeLa cells after 3 hours of starvation. (E) Quantitation of the percentage of PLA dots that co-localize with each indicated organelle marker. Bars represent mean values ± SEM for three different experiments (each value represents percentage of PLA dots at indicated organelle using total number of PLA dots in >100 cells analyzed as the denominator). WCL, whole cell lysate. Scale bars, 10 μm. $^{**}P < 0.01$, $^{***}P < 0.001$, Two-way ANOVA (C).

Figure 2. Beclin 1 and Na^+,K^+-ATPase interact in mouse and human tissues during starvation. (A-D) Representative western blots (A, C) and quantitation (B, D) of Na^+,K^+-ATPase co-immunoprecipitation with Beclin 1 from hearts (A, B) and livers (C, D) of mice after normal feeding or 48 hours of starvation. For (A) and (C), the same tissue sample of the non-starved group in lane 1 of the gel was used as a control for IgG immunoprecipitation. In (B) and (D), bars represent mean ± SD (n =

10 mice). (E, F) Representative images (E) and quantitation (F) of proximity ligase assay of Beclin 1 and Na^+,K^+-ATPase in the indicated tissue and condition. For (F), bars represent mean ± SEM (n = 10 mice, 10 randomly selected fields analyzed per mouse). (G, H) Representative images (G) and quantitation (H) of proximity ligation assay of Beclin 1 and the α-subunit of Na^+,K^+-ATPase in livers from normal subjects (Control, Ctrl) or patients with anorexia nervosa (AN). In (H), bars represent mean ± SEM (n = 3 patients, at least 5 randomly selected fields analyzed per patient sample). *, non-specific band: WCL, whole cell lysate. Scale bars, 50 μm. $^{**}P < 0.01$, $^{***}P < 0.001$, Two-way ANOVA test (F) and two-tailed unpaired Student's t-test (B, D, H).

Figure 3. Beclin 1 and Na^+,K^+-ATPase interact in vivo during cerebral hypoxic-ischemia and renal ischemic reperfusion injury. (A, B) Representative western blots (A) and quantitation (B) of co-immunoprecipitation of Beclin 1 with the α-subunit of Na^+,K^+-ATPase in the hippocampus of rat pups that were sacrificed 6 hours after receiving intraperitoneal vehicle or neriifolin (0.22 mg/kg) and subjected to sham operations or cerebral hypoxia-ischemia (HI). In (B), bars represent mean ± SD (n = 3 rats per group). (C, D) Representative images (C) and quantitation (D) of proximity ligation assays (PLA) of Beclin 1 and the α-subunit of Na^+,K^+-ATPase in the CA3 hippocampal region of rat pups that were sacrificed 6 hours after receiving intraperitoneal vehicle or neriifolin (0.22 mg/kg) and subjected to sham operations or cerebral HI. In (D), bars represent mean ± SEM (n = 5 rats per group, 4 randomly selected fields analyzed per animal). (E, F) Representative western blots (E) and quantitation (F) of co-immunoprecipitation of Beclin 1 with the α-subunit of Na^+,K^+-ATPase in kidneys from mice that were subjected to sham operations or renal ischemia-reperfusion injury (IRI) after peritoneal administration with either vehicle or ouabain (0.25 mg/kg). In (F) bars represent mean ± SD (n = 3 mice per group). (G, H) Representative images (G) and quantitation (H) of proximity ligation assays of Beclin 1 and the α-

subunit of Na^+,K^+-ATPase in kidneys from mice that were subjected to sham operations or renal IRI after peritoneal administration with either vehicle or ouabain (0.25 mg/kg). In (H) bars represent mean ± SEM (n = 5-7 mice per group; 10 randomly selected fields analyzed per mouse). For (A) and (E), the same tissue sample of the sham group (lane 1 of gel) was used as a control for IgG immunoprecipitation. *, non-specific band: WCL, whole cell lysate. Scale bars, 10 μm (C) and 50 μm (G). $*P < 0.05$, $**P < 0.01$, $***P < 0.001$; One-way (B, D) and two-way (F, H) ANOVA test.

Figure 4. Ouabain decreases autotic cell death and improves outcome in renal ischemia reperfusion injury. (A, B) Representative micrographs (A) and quantitation (B) of autotic pericytes in the kidneys from mice that were subjected to sham operations or renal ischemia-reperfusion injury (IRI) after peritoneal administration of either vehicle or ouabain (0.25 mg/kg). In (B), bars represent mean ± SEM (n = 5-8 mice per group; more than 50 cells analyzed per mouse). (C, D) Representative H&E images (C) and histological score (D) of kidneys from mice that were subjected to sham operations or renal IRI after peritoneal administration of either vehicle or ouabain (0.25 mg/kg). In (D), bars represent mean ± SEM. (n = 5-8 mice per group; 10 randomly selected fields analyzed per mouse). (E, F) Assessment of renal damage as measured by blood urea nitrogen (BUN) (E) and creatinine (F) levels in plasma from mice that were subjected to sham operations or renal IRI after peritoneal administration of either vehicle or ouabain (0.25 mg/kg). Bars represent mean ± SD (n = 5-8 mice per group). Scale bars, 1 μm (A) and 50 μm (C). $**P < 0.01$; $***P < 0.001$; Two-way ANOVA test.

Figure 5. Endogenous cardiac glycosides regulate Beclin 1/Na^+,K^+-ATPase binding and autosis during exercise. (A, B) Representative western blots (A) and quantitation (B) of co-immunoprecipitation of Beclin 1 with the α-subunit of Na^+,K^+-ATPase in hearts from mice treated with

either intraperitoneal vehicle or cardiac glycoside blocking antibody DigiFab (10 mg/kg) before 80 minutes of resting or exercise. For (A), the same issue sample of the resting group without DigiFab (lane 1) was used as a control for IgG immunoprecipitation. In (B), bars represent mean ± SD (n = 10 mice per group). (C, D) Representative images (C) and quantitation (D) of proximity ligation assays (PLA) of Beclin 1 and the α-subunit of Na^+,K^+-ATPase in hearts from mice treated with either intraperitoneal vehicle or cardiac glycoside blocking antibody DigiFab (10 mg/kg) before 80 minutes of resting or exercise. In (D), bars represent mean ± SEM (n = 6-8 mice per group; 10 randomly selected fields analyzed per mouse). (E, F) Representative micrographs (E) and quantitation (F) of autotic non-cardiomyocyte cells in hearts from mice treated with either intraperitoneal vehicle or cardiac glycoside blocking antibody DigiFab (10 mg/kg) before resting or running until exhaustion. In (F), bars represent mean ± SEM (n = 6 randomly selected areas from a total of 3 mice per condition, more than 1,000 analyzed cells per area). *, non-specific band: WCL, whole cell lysate. Scale bars, 10 μm (B) and 1 μm (C). *$P < 0.05$, **$P < 0.01$, ***$P < 0.001$; Two-way ANOVA test.

Supplemental Figure 1. Identification of autosis regulators in a genome-wide siRNA screen. (A, B), Schematic diagrams of genome-wide siRNA screening for regulators of Tat-Beclin 1-induced autosis. See Materials and Methods for details. (C), Ranked distribution of z-score averages for each siRNA pool in primary genome-wide siRNA screen. See Supplemental Table 1 for top hits from primary screen, Supplemental Table 2 for top hits from conformational screen and Supplemental Table 3 for top hits from the final deconvolution screen. All assays were performed in triplicate.

Supplemental Figure 2. Beclin 1 and Na^+,K^+-ATPase interact during autophagy-inducing peptide treatment. (A) Co-immunoprecipitation of Beclin 1 with the α-subunit of Na^+,K^+-ATPase in HeLa cells

after 3 hours of treatment with Tat-Scrambled peptide or Tat-Beclin 1 active peptide supplemented with either vehicle or 10 μM digoxin. The same cell lysate from cells treated with Tat-Scrambled peptide was used as a control for IgG immunoprecipitation. Similar results were observed in three independent experiments. (B, C) Representative images (B) and quantitation (C) of proximity ligase assay (PLA) of Beclin 1 and Na^+,K^+-ATPase in the indicated conditions. In (C) mean values ± SEM from three independent experiments (value for each experiment represent mean value of at least 100 cells per condition). Scale bars, 10 μm. $^{**}P < 0.01$, Two-way ANOVA test.

Supplemental Figure 3. Increased interaction between Beclin 1 and Na^+,K^+-ATPase during autosis but not apoptosis. (A) Representative images of differential interference contrast (DIC) microscopy and proximity ligation assays (PLA) of Beclin 1 and Na^+,K^+-ATPase in apoptotic and autotic-like HeLa cells after 24 hours of starvation. Apoptotic cells were defined as those cells with rounded morphology and cytoplasmic and cell surface blebbing. Autotic-like cells were defined as cells with perinuclear ballooning. (B), Quantitation of (A). Bars represent mean ± SD (n = 13 cells per condition). $^{***}P < 0.001$; One-tailed unpaired Student's t-test.

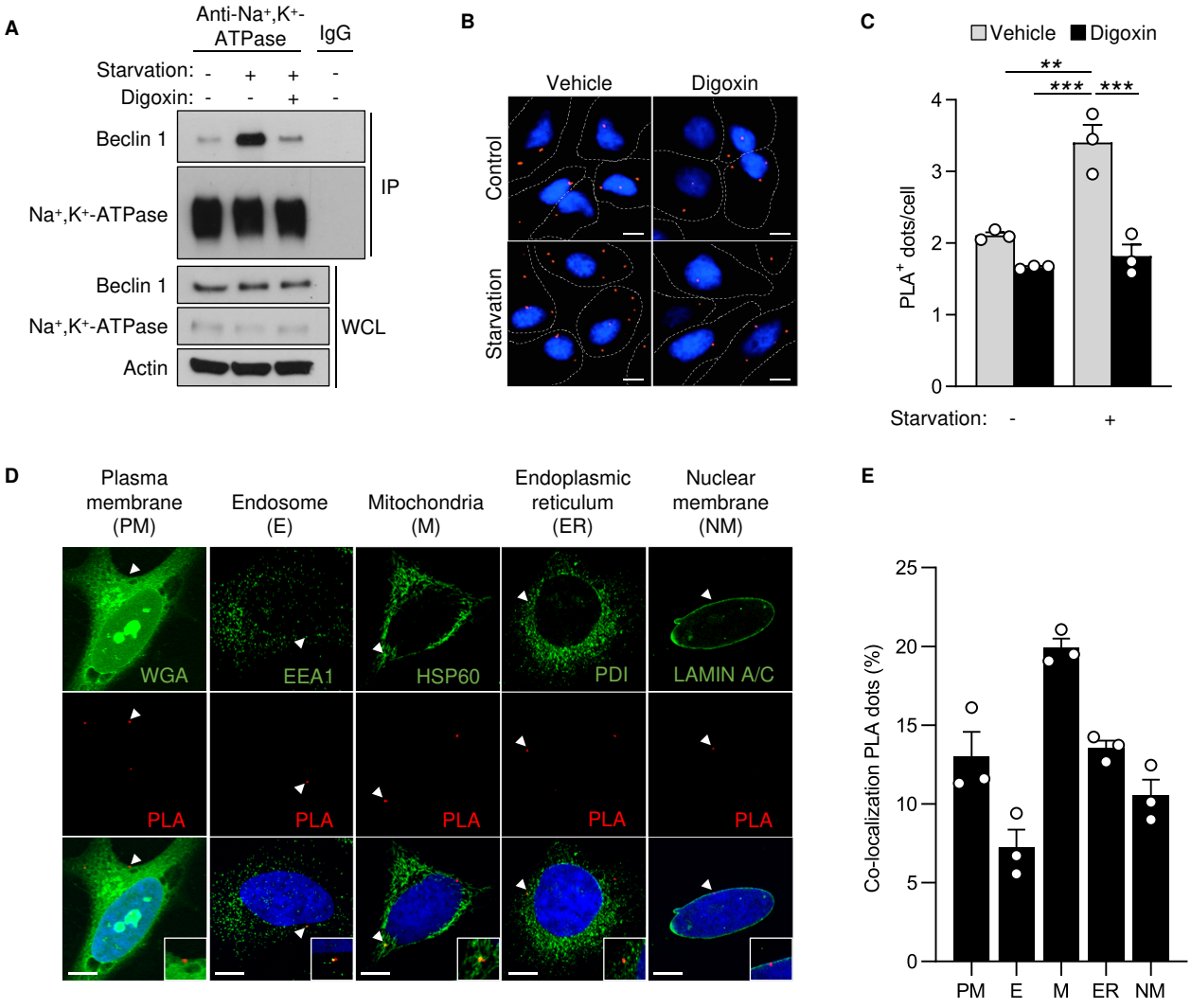

Figure 1. Beclin 1 and Na⁺,K⁺-ATPase interact in cultured cells during starvation. (A) Co-immunoprecipitation of Beclin 1 with Na⁺,K⁺-ATPase in HeLa cells after 3 hours of growth in normal media (-) or HBSS starvation media (+) treated with either vehicle or 10 μM digoxin. The same lysate from cells grown in normal media without digoxin (lane 1) was used as a control for IgG immunoprecipitation. Similar results were observed in three independent experiments. (B, C) Representative images (B) and quantitation (C) of proximity ligase assay (PLA) of Beclin 1 and Na⁺,K⁺-ATPase in the indicated conditions. In (C), bars represent mean values ± SEM from three independent experiments (value for each experiment represent mean value of at least 100 cells per condition). (D) Representative images of proximity ligation assays (PLA) of Beclin 1 and Na⁺,K⁺-ATPase co-stained with markers of plasma membrane (wheat germ agglutinin, WGA), endosomes (EEA1), mitochondria (HSP60), endoplasmic reticulum (PDI) and nuclear membrane (LAMIN A/C) in HeLa cells after 3 hours of starvation. (E) Quantitation of the percentage of PLA dots that co-localize with each indicated organelle marker. Bars represent mean values ± SEM for three different experiments (each value represents percentage of PLA dots at indicated organelle using total number of PLA dots in >100 cells analyzed as the denominator). WCL, whole cell lysate. Scale bars, 10 μm. **P < 0.01, ***P < 0.001, Two-way ANOVA (C).

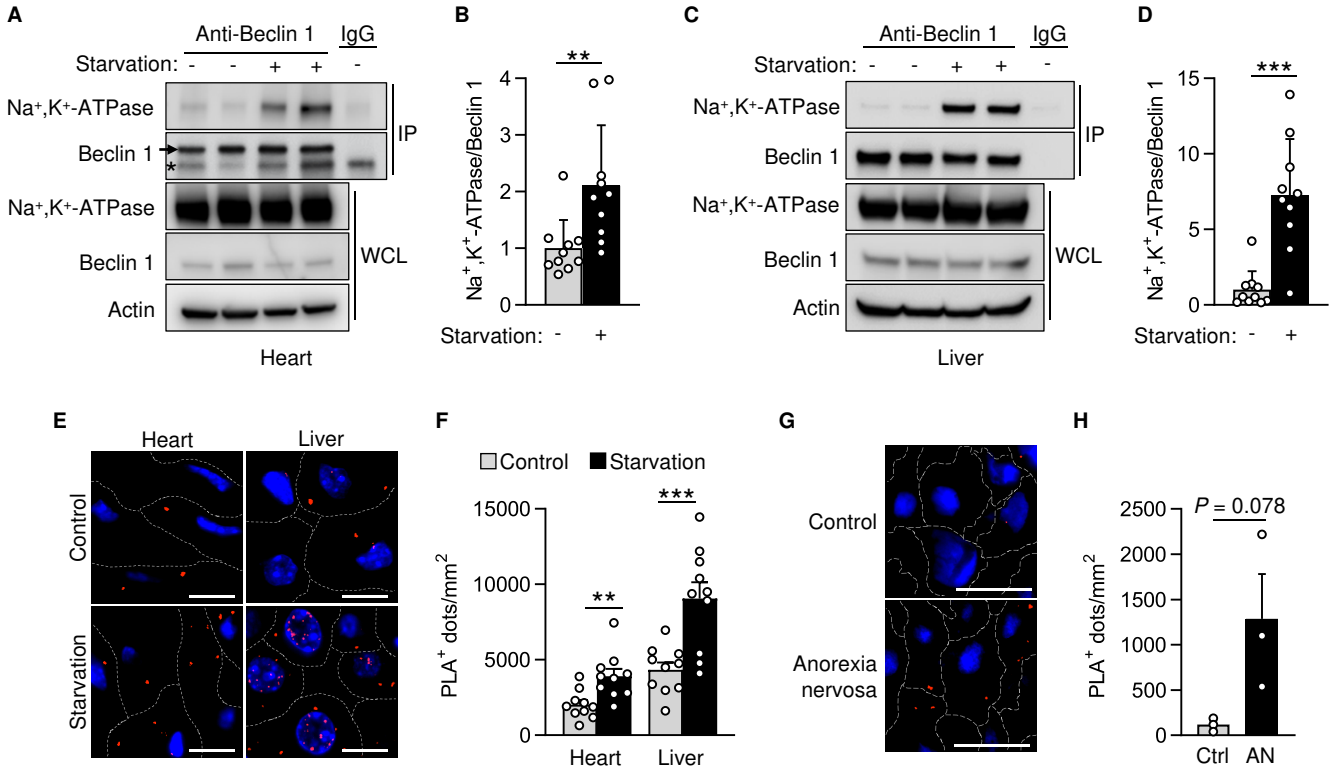

Figure 2. Beclin 1 and Na⁺,K⁺-ATPase interact in mouse and human tissues during starvation. (A-D) Representative western blots (A, C) and quantitation (B, D) of Na⁺,K⁺-ATPase co-immunoprecipitation with Beclin 1 from hearts (A, B) and livers (C, D) of mice after normal feeding or 48 hours of starvation. For (A) and (C), the same tissue sample of the non-starved group in lane 1 of the gel was used as a control for IgG immunoprecipitation. In (B) and (D), bars represent mean ± SD (n = 10 mice). (E, F) Representative images (E) and quantitation (F) of proximity ligase assay of Beclin 1 and Na⁺,K⁺-ATPase in the indicated tissue and condition. For (F), bars represent mean ± SEM (n = 10 mice, 10 randomly selected fields analyzed per mouse). (G, H) Representative images (G) and quantitation (H) of proximity ligation assay of Beclin 1 and Na⁺,K⁺-ATPase in livers from normal subjects (Control, Ctrl) or patients with anorexia nervosa (AN). In (H), bars represent mean ± SEM (n = 3 patients, at least 5 randomly selected fields analyzed per patient sample). *, non-specific band: WCL, whole cell lysate. Scale bars, 50 μm. **P < 0.01, ***P < 0.001, Two-way ANOVA test (F) and two-tailed unpaired Student's t-test (B, D, H).

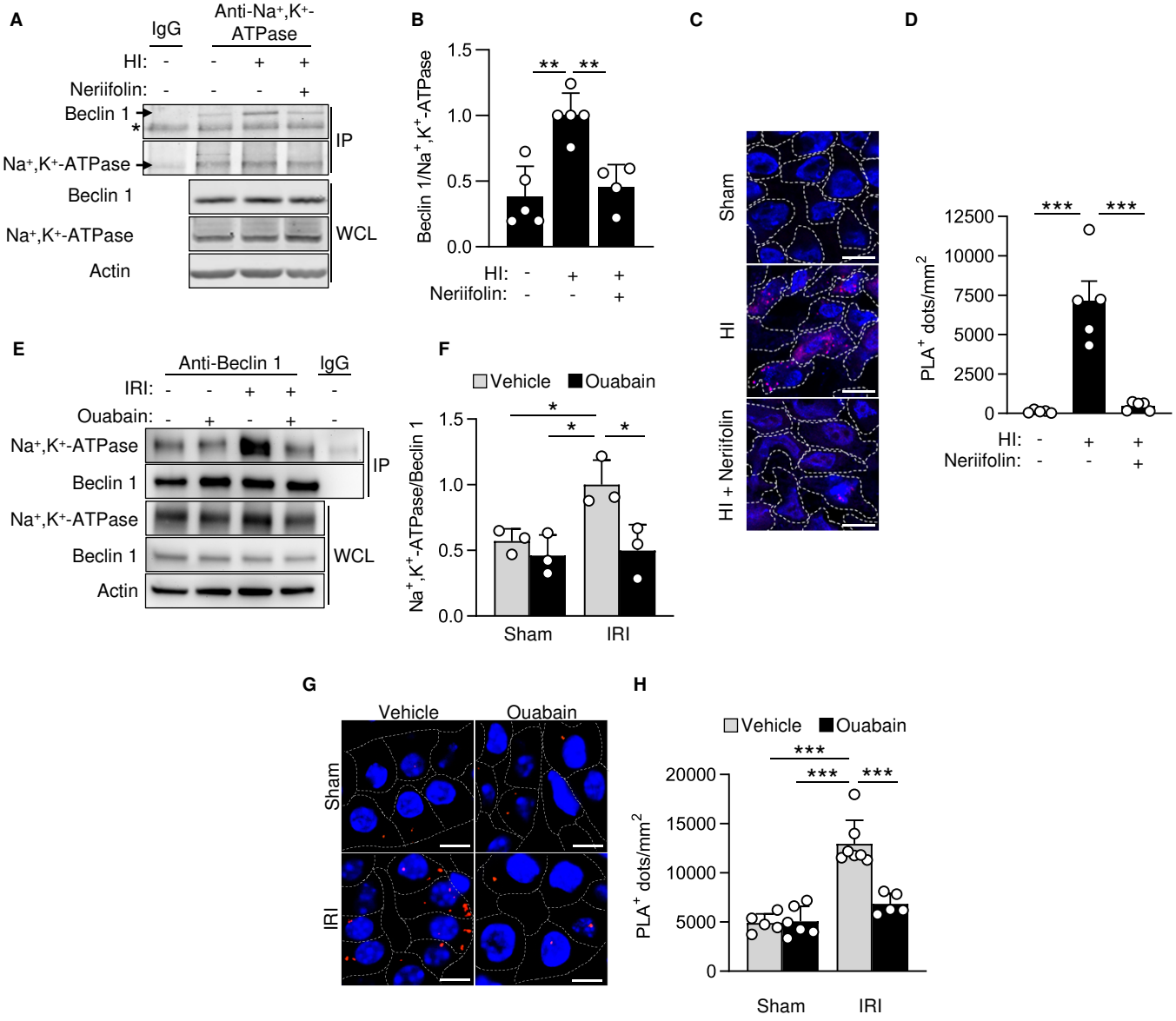

Figure 3. Beclin 1 and Na⁺,K⁺-ATPase interact in vivo during cerebral hypoxic-ischemia and renal ischemic reperfusion injury. (A, B) Representative western blots (A) and quantitation (B) of co-immunoprecipitation of Beclin 1 with Na⁺,K⁺-ATPase in the hippocampus of rat pups that were sacrificed 6 hours after receiving intraperitoneal vehicle or neriifolin (0.22 mg/kg) and subjected to sham operations or cerebral hypoxia-ischemia (HI). In (B), bars represent mean ± SD (n = 3 rats per group). (C, D) Representative images (C) and quantitation (D) of proximity ligation assays (PLA) of Beclin 1 and Na⁺,K⁺-ATPase in the CA3 hippocampal region of rat pups that were sacrificed 6 hours after receiving intraperitoneal vehicle or neriifolin (0.22 mg/kg) and subjected to sham operations or cerebral HI. In (D), bars represent mean ± SEM (n = 5 rats per group, 4 randomly selected fields analyzed per animal). (E, F) Representative western blots (E) and quantitation (F) of co-immunoprecipitation of Beclin 1 with Na⁺,K⁺-ATPase in kidneys from mice that were subjected to sham operations or renal ischemia-reperfusion injury (IRI) after peritoneal administration with either vehicle or ouabain (0.25 mg/kg). In (F) bars represent mean ± SD (n = 3 mice per group). (G, H) Representative images (G) and quantitation (H) of proximity ligation assays of Beclin 1 and Na⁺,K⁺-ATPase in kidneys from mice that were subjected to sham operations or renal IRI after peritoneal administration with either vehicle or ouabain (0.25 mg/kg). In (H) bars represent mean ± SEM (n = 5-7 mice per group; 10 randomly selected fields analyzed per mouse). For (A) and (E), the same tissue sample of the sham group (lane 1 of gel) was used as a control for IgG immunoprecipitation. *, non-specific band: WCL, whole cell lysate. Scale bars, 10 μm (C) and 50 μm (G). *P < 0.05, **P < 0.01, ***P < 0.001; One-way (B, D) and two-way (F, H) ANOVA test

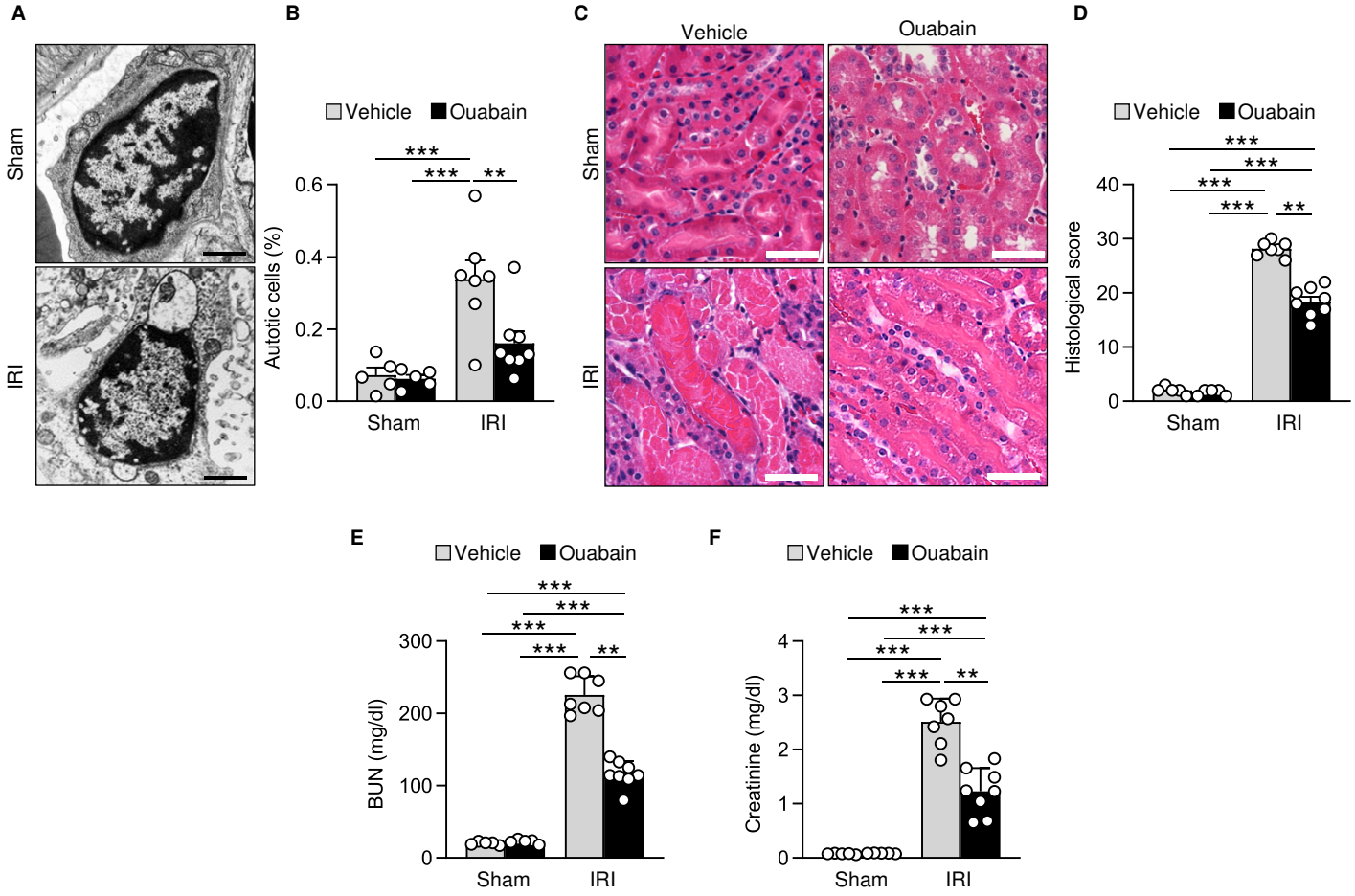

Figure 4. Ouabain decreases autotic cell death and improves outcome in renal ischemia reperfusion injury. (A, B) Representative micrographs (A) and quantitation (B) of autotic pericytes in the kidneys from mice that were subjected to sham operations or renal ischemia-reperfusion injury (IRI) after peritoneal administration of either vehicle or ouabain (0.25 mg/kg). In (B), bars represent mean ± SEM (n = 5-8 mice per group; more than 50 cells analyzed per mouse). (C, D) Representative H&E images (C) and histological score (D) of kidneys from mice that were subjected to sham operations or renal IRI after peritoneal administration of either vehicle or ouabain (0.25 mg/kg). In (D), bars represent mean ± SEM. (n = 5-8 mice per group; 10 randomly selected fields analyzed per mouse). (E, F) Assessment of renal damage as measured by blood urea nitrogen (BUN) (E) and creatinine (F) levels in plasma from mice that were subjected to sham operations or renal IRI after peritoneal administration of either vehicle or ouabain (0.25 mg/kg). Bars represent mean ± SD (n = 5-8 mice per group). Scale bars, 1 μm (A) and 50 μm (C). $^{**}P < 0.01$; $^{***}P < 0.001$; Two-way ANOVA test.

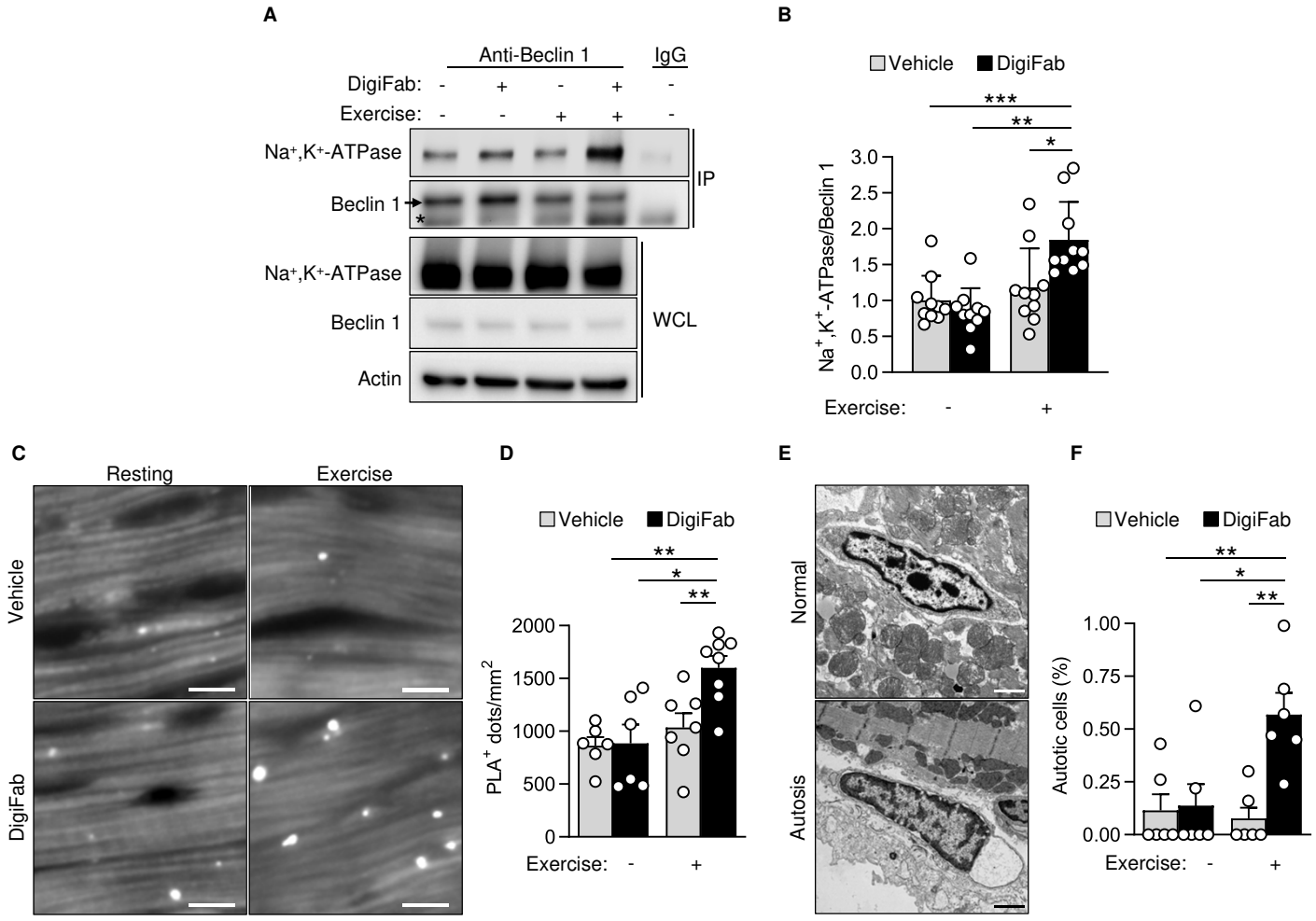

Figure 5. Endogenous cardiac glycosides regulate Beclin 1/Na⁺,K⁺-ATPase binding and autosis during exercise. (A, B) Representative western blots (A) and quantitation (B) of co-immunoprecipitation of Beclin 1 with the α-subunit of Na⁺,K⁺-ATPase in hearts from mice treated with either intraperitoneal vehicle or cardiac glycoside blocking antibody DigiFab (10 mg/kg) before 80 minutes of resting or exercise. For (A), the same issue sample of the resting group without Digifab (lane 1) was used as a control for IgG immunoprecipitation. In (B), bars represent mean ± SD (n = 10 mice per group). (C, D) Representative images (C) and quantitation (D) of proximity ligation assays (PLA) of Beclin 1 and the α-subunit of Na⁺,K⁺-ATPase in hearts from mice treated with either intraperitoneal vehicle or cardiac glycoside blocking antibody DigiFab (10 mg/kg) before 80 minutes of resting or exercise. In (D), bars represent mean ± SEM (n = 6-8 mice per group; 10 randomly selected fields analyzed per mouse). (E, F) Representative micrographs (E) and quantitation (F) of autotic non-cardiomyocyte cells in hearts from mice treated with either intraperitoneal vehicle or cardiac glycoside blocking antibody DigiFab (10 mg/kg) before resting or running until exhaustion. In (F), bars represent mean ± SEM (n = 6 randomly selected areas from a total of 3 mice per condition, more than 1,000 analyzed cells per area). *, non-specific band: WCL, whole cell lysate. Scale bars, 10 μm (B) and 1 μm (C). $^{*}P < 0.05$, $^{**}P < 0.01$, $^{***}P < 0.001$; Two-way ANOVA test.

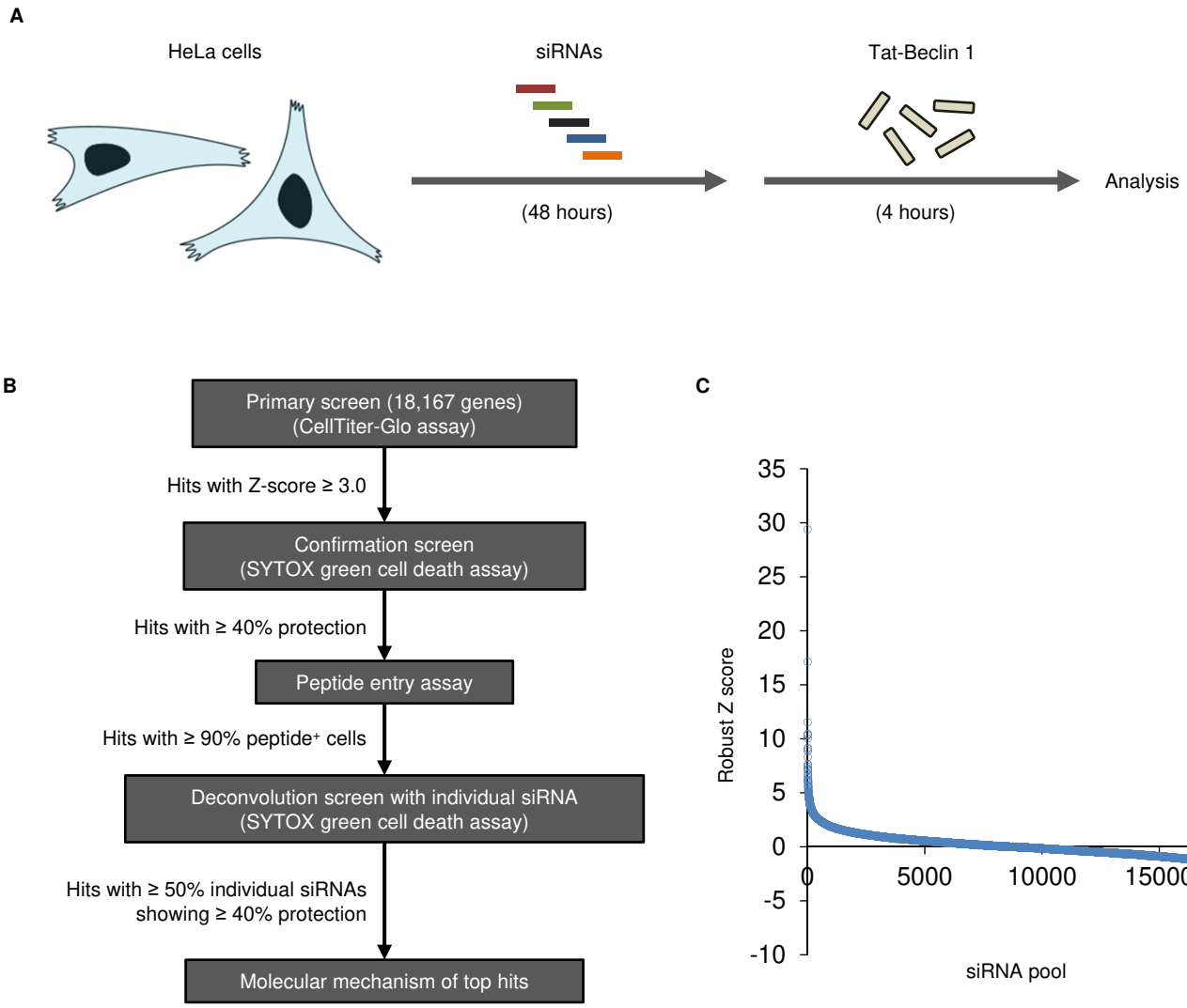

Supplemental Figure 1. Identification of autosis regulators in a genome-wide siRNA screen. (A, B), Schematic diagrams of genome-wide siRNA screening for regulators of Tat-Beclin 1-induced autosis. See Methods for details. (C), Ranked distribution of z-score averages for each siRNA pool in primary genome-wide siRNA screen. See Supplemental Table 1 for top hits from primary screen, Supplemental Table 2 for top hits from conformational screen and Supplemental Table 3 for top hits from the final deconvolution screen. All assays were performed in triplicate.

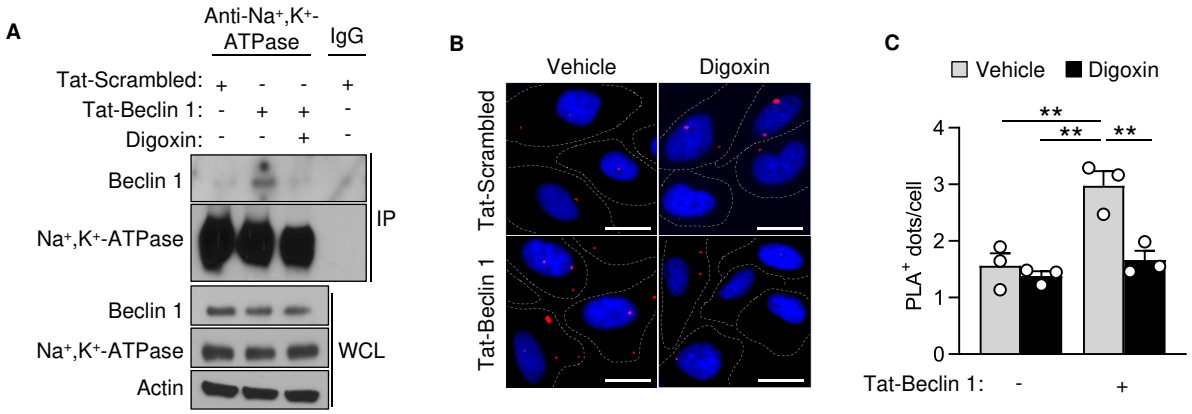

Supplemental Figure 2. Beclin 1 and Na⁺,K⁺-ATPase interact during autophagy-inducing peptide treatment. (A) Co-immunoprecipitation of Beclin 1 with the α-subunit of Na⁺,K⁺-ATPase in HeLa cells after 3 hours of treatment with Tat-Scrambled peptide or Tat-Beclin 1 active peptide supplemented with either vehicle or 10 μM digoxin. The same cell lysate from cells treated with Tat-Scrambled peptide was used as a control for IgG immunoprecipitation. Similar results were observed in three independent experiments. (B, C) Representative images (B) and quantitation (C) of proximity ligase assay (PLA) of Beclin 1 and the α-subunit of Na⁺,K⁺-ATPase in the indicated conditions. In (C) mean values ± SEM from three independent experiments (value for each experiment represent mean value of at least 100 cells per condition). Scale bars, 10 μm. $^{**}P < 0.01$, Two-way ANOVA test.

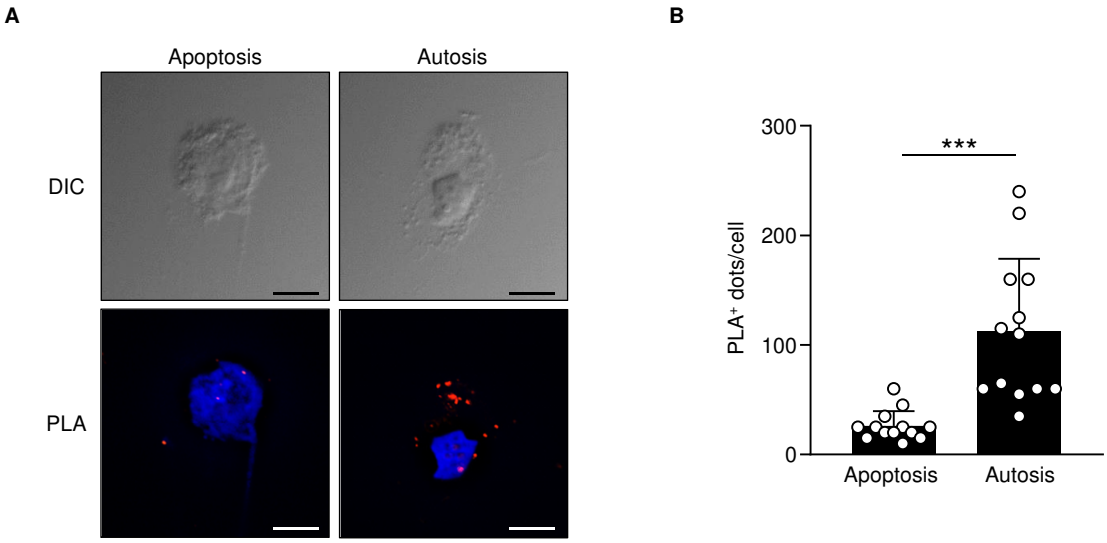

Supplemental Figure 3. Increased interaction between Beclin 1 and Na^+,K^+-ATPase during autosis but not apoptosis. (A) Representative images of differential interference contrast (DIC) microscopy and proximity ligation assays (PLA) of Beclin 1 and Na^+,K^+-ATPase in apoptotic and autotic-like HeLa cells after 24 hours of starvation. Apoptotic cells were defined as those cells with rounded morphology and cytoplasmic and cell surface blebbing. Autotic-like cells were defined as cells with perinuclear ballooning. (B), Quantitation of (A). Bars represent mean ± SD (n = 13 cells per condition). ***$P < 0.001$; Two-tailed unpaired Student's t-test.

Supplemental Table 1: Top hits from primary screen

Symbol	Name	Function	Average Z-scores
ATP1A1	ATPase Na+/K+ transporting subunit alpha 1	Component of ion pump	25.151
TRIM25	tripartite motif containing 25	E3 ubiquitin ligase in immunity	17.780
ZNF185	zinc finger protein 185 with LIM domain	Cytoskeleton dynamics	11.798
RFWD3	ring finger and WD repeat domain 3	E3 ubiquitin ligase in DNA repair	10.259
WFDC1	WAP four-disulfide core domain 1	Control of stromal-epithelial interaction	10.250
KCNN4	potassium calcium-activated channel subfamily N member 4	Component of ion channel	9.090
SOAT2	sterol O-acyltransferase 2	Acyl-CoA:cholesterol acyltransferase	9.044
RNASET2	ribonuclease T2	Lysosomal degradation of RNA	8.566
ACP5	acid phosphatase type 5. tartrate resistant	Dephosphorylation of osteopontin	8.380
KCNQ2	potassium voltage-gated channel subfamily Q member 2	Component of ion channel	8.120
SAMD4	sterile alpha motif domain containing 4	RNA-binding post-transcriptional regulator	8.054
TMEM132E	transmembrane protein 132E	Cellular adhesion	7.837
PPFIA3	PTPRF interacting protein alpha 3	Regulation of focal adhesions	7.370
AIRE	autoimmune regulator	Transcription factor in T cell negative selection	7.324
TRIM46	tripartite motif containing 46	Microtubule organization in neuronal polarization	7.095
MEX3B	mex-3 RNA binding family member B	RNA-binding post-transcriptional regulator	7.053
ECEL1	endothelin converting enzyme like 1	Endopeptidase in regulation of neuropeptides	6.865
MRPL22	mitochondrial ribosomal protein L22	Mitochondrial protein synthesis	6.790
IFNAR1	Interferon alpha and beta receptor subunit 1	Receptor for IFN-alpha and IFN-beta	6.787
PTPNS1 (SIRPA)	signal regulatory protein alpha	Inhibitory receptor of CD47	6.769
PVRL4 (NECTIN4)	nectin cell adhesion molecule 4	Regulation of cadherin-based adherens junctions	6.750
PPP1R14A	protein phosphatase 1 regulatory inhibitor subunit 14A	Smooth muscle contraction	6.578
PABPC1	poly(A) binding protein cytoplasmic 1	mRNA regulation	6.412
SYS1	SYS1 golgi trafficking protein	Targeting of ARFRP1 to the Golgi apparatus	6.264
AQP2	aquaporin 2	Renal water homeostasis	5.919
SSX6	SSX family member 6. pseudogene	Probable transcriptional repressor	5.867
HECTD1	HECT domain E3 ubiquitin protein ligase 1	E3 ubiquitin ligase in different processes	5.712
LDAH	lipid droplet associated hydrolase	Lipid hydrolase involved in triacylglycerol dynamics	5.599
PTPRN2	protein tyrosine phosphatase receptor N2	Phosphatidylinositol phosphatase in insulin secretion	5.531
RAB40AL	RAB40A like	Protein targeting for proteasomal degradation	5.498
TRAF3	TNF receptor associated factor 3	Signal transducer of different immune receptors	5.465
MIB1	mindbomb E3 ubiquitin protein ligase 1	E3 ubiquitin ligase in different processes	5.259
G3BP1	GRBP stress granule assembly factor 1	Helicase in DNA sensing; stress granule assembly	5.239
SSX2	SSX family member 2	Probable transcriptional repressor	5.218
TRIM56	tripartite motif containing protein 56	E3 ubiquitin ligase in immunity	5.164
COQ10B	coenzyme Q10B	Coenzyme Q chaperone	5.161
ZFH4	zinc finger homeobox 4	Transcription factor in neural cell differentiation	5.117
ZNF278 (PATZ1)	POZ/BTB and AT hook containing zinc finger 1	Transcriptional repressor	5.111
CCNE2	cyclin-E2	Cell cycle regulation	5.022

Supplemental Table 2: Top hits from confirmation screen

Symbol	Name	Function	Cell death protection (%)
ATP1A1	ATPase Na+/K+ transporting subunit alpha 1	Component of ion pump	118.27%
HIST1H2AI (H2AC13)	H2A clustered histone 13	Core component of nucleosome	106.19%
CBX1	chromobox 1	Epigenetic repression in heterochromatin	103.03%
IGSF9	Immunoglobulin superfamily 9	Cell adhesion molecule in synapses	92.01%
STAU2	staufen double-stranded RNA binding protein 2	mRNA transport in heart and brain	88.52%
ARSI	arylsulfatase family member I	Hydrolysis of sulfate esters	87.42%
FLJ40142	Unknown	Unknown	87.10%
RNASET2	ribonuclease T2	Lysosomal degradation of RNA	87.00%
SYT9	synaptotagmin 9	Ca2+-dependent exocytosis	85.77%
WFDC1	WAP four disulfide core domain 1	Control of stromal-epithelial interaction	82.88%
SAMD4	sterile alpha motif domain containing 4	RNA-binding post-transcriptional regulator	80.78%
SYS1	SYS1 golgi trafficking protein	Targeting of ARFRP1 to the Golgi apparatus	80.41%
TRIM25	tripartite motif containing 25	E3 ubiquitin ligase in immunity	80.12%
ATP2B2	ATPase plasma membrane Ca2+ transporting 2	Transport of calcium	71.78%
EVPL	evnoplakin	Cytoskeletal linker protein	69.27%
PPFIA3	PTPRF interacting protein alpha 3	Regulation of focal adhesions	68.84%
SLC6A8	solute carrier family 6 member 8	Creatine transporter	66.42%
THBS3	thrombospondin 3	Cell-to-cell. cell-to-matrix interactions	65.17%
TRPT1	tRNA phosphotransferase 1	tRNA splicing	64.27%
TMEM132E	transmembrane protein 132E	Cellular adhesion	63.60%
HIST1H2BL (H2BC13)	H2B clustered histone 13	Core component of nucleosome	63.34%
SLC22A5	solute carrier family 22 member 5	Carnitine transporter	61.85%
MRPL22	mitochondrial ribosomal protein L22	Mitochondrial protein synthesis	60.55%
RAB40L	RAB40A	Protein targeting for proteasomal degradation	60.48%
AQP2	aquaporin-2	Renal water homeostasis	57.45%
PGLYRP3	peptidoglycan recognition protein 3	Antimicrobial peptide	57.28%
VPS28	VPS28 subunit of ESCRT-I	Vesicular trafficking	55.45%
HES2	hes family bHLH transcription factor 2	Transcriptional repressor	54.81%
NFKBIZ	NFKB inhibitor zeta	Nuclear inhibitor of NF-kB	54.57%
PPP1R3A	protein phosphatase 1 regulatory subunit 3A	Regulation of PP1 in muscle	53.51%
PSCD2 (CYTH2)	cytohesin 2	Activator of Arf-family small GTPases	53.18%
SLCO4A1	solute carrier organic anion transporter family 4A1	Transport of organic anions	52.98%
TM4SF5	transmembrane 4 L six family member 5	Lysosomal arginine sensor. mTORC1 activator	52.50%
AIRE	autoimmune regulator	Transcription factor in T cell negative selection	52.07%
MCMDC1 (MCM9)	minichromosome maintenance 9 homologous recombination repair factor	Repair of double-stranded DNA breaks and DNA interstrand cross-links	51.30%
TDRD3	tudor domain containing 3	Methylarginine recognition	50.62%
DRD4	dopamine receptor D4	Dopamine receptor in many processes	50.11%

Supplemental Table 3: Top hits from deconvolution screen

Symbol	Name	Function	% Dharmacon siRNA (Total = 4)	% Invitrogen siRNA (Total = 3)
ATP1A1	ATPase Na+/K+ transporting subunit alpha 1	Component of ion pump	100%	100%
KCNN4	potassium calcium-activated channel subfamily N member 4	Component of ion channel	100%	67%
NICN1	nicolin 1	Nuclear protein of unknown function	50%	100%
SAMD4A	sterile alpha motif domain containing 4	RNA-binding post-transcriptional regulator	75%	67%
SPG7	SPG7 matrix AAA peptidase subunit, paraplegin	Mitochondrial metalloprotease (AAA protein family)	50%	100%
ARSI	arylsulfatase I	Hydrolysis of sulfate esters	75%	33%
CSPP1	centrosome and spindle pole associated protein 1	Cell-cycle progression; cilia formation	75%	33%
ADGRF1	adhesion G protein-coupled receptor F1	Adhesion-GPCR involved in brain development	50%	67%
KCNQ2	potassium voltage-gated channel subfamily Q member 2	Component of ion channel	75%	33%
SYS1	SYS1 golgi trafficking protein	Targeting of ARFRP1 to the Golgi apparatus	75%	33%
RAB40AL	Ras-related protein Rab-40A-like	Protein targeting for proteasomal degradation	75%	0%
THBS3	thrombospondin 3	Cell-to-cell, cell-to-matrix interactions	75%	0%
TRPT1	tRNA 2'-phosphotransferase 1	tRNA splicing	75%	0%

Full unedited gels for Figure 1A

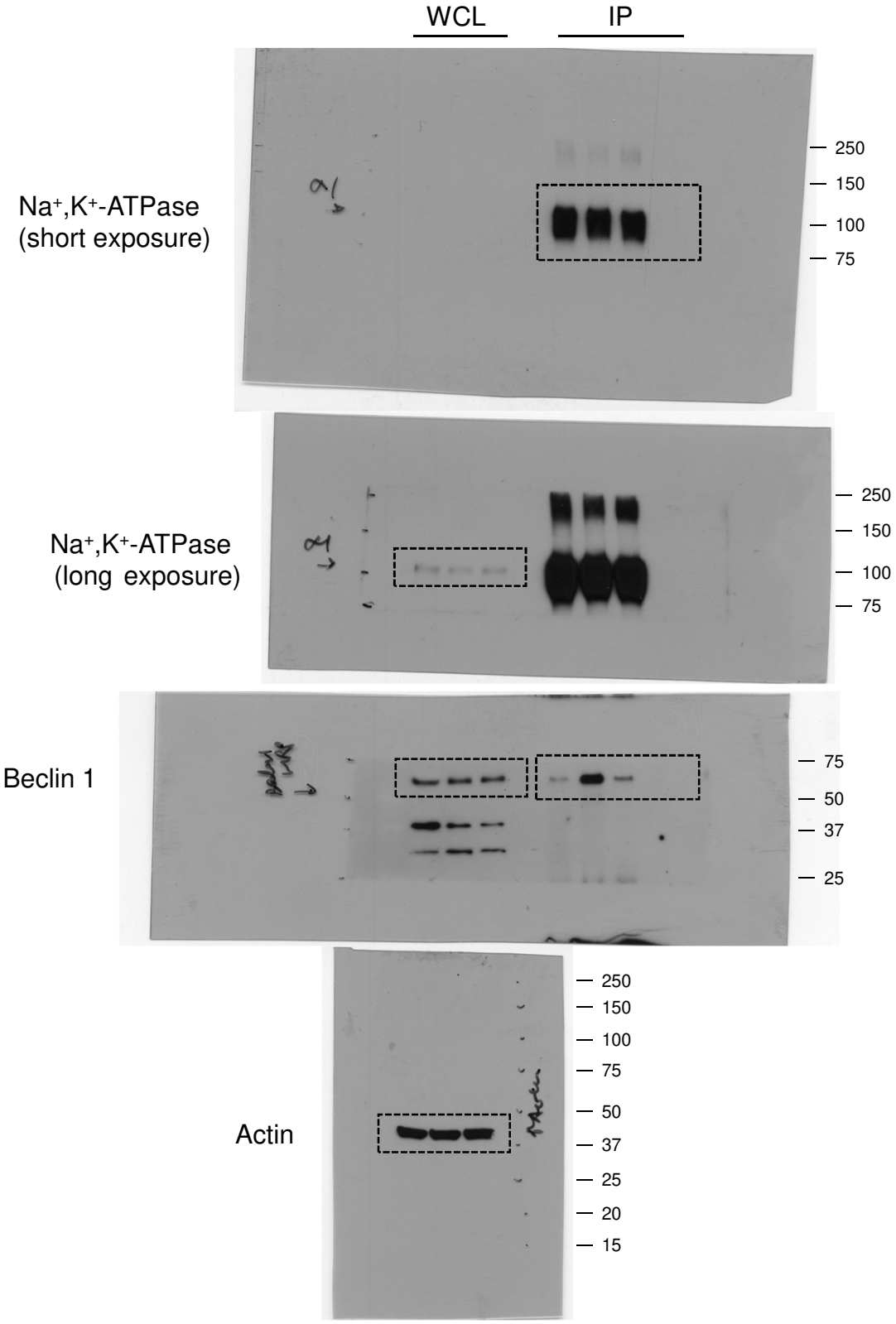

Full unedited gels for Figure 2A

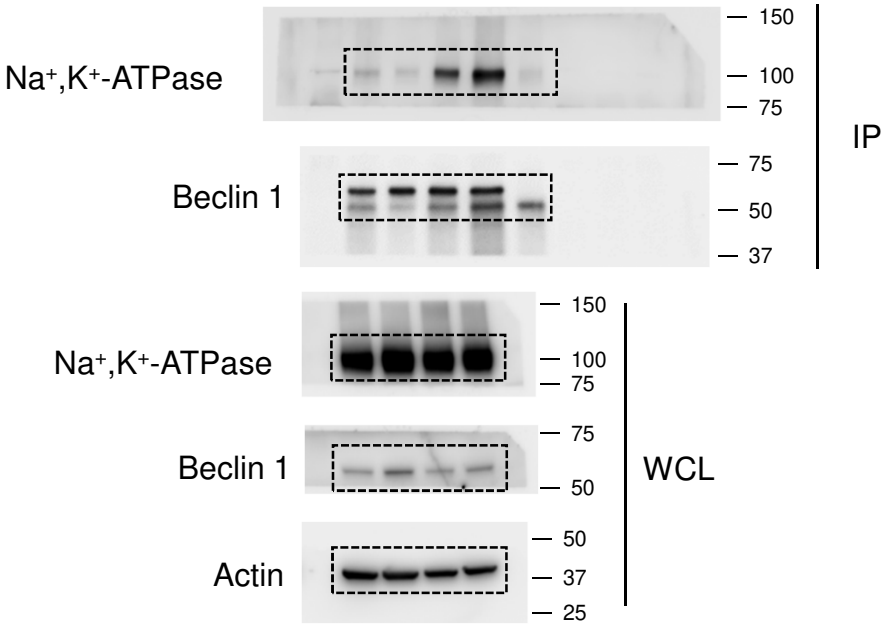

Full unedited gels for Figure 2C

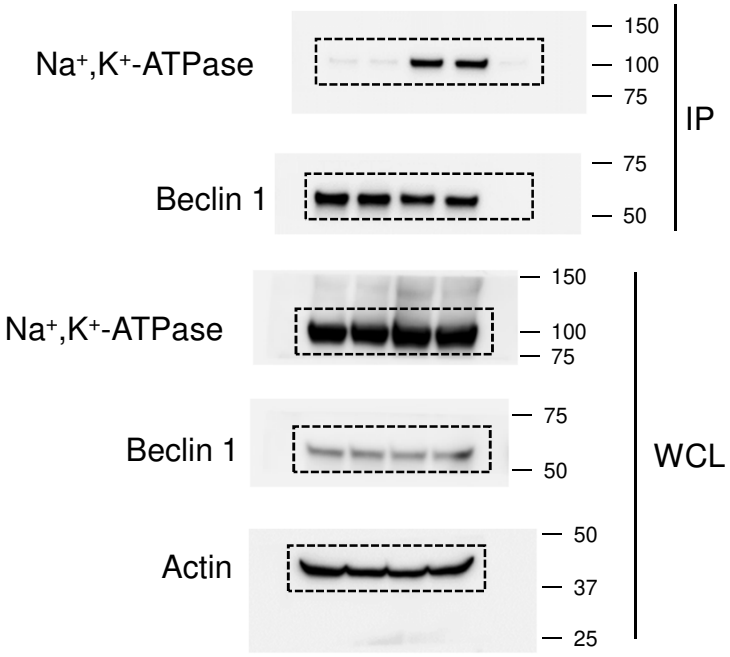

Full unedited gels for Figure 3A

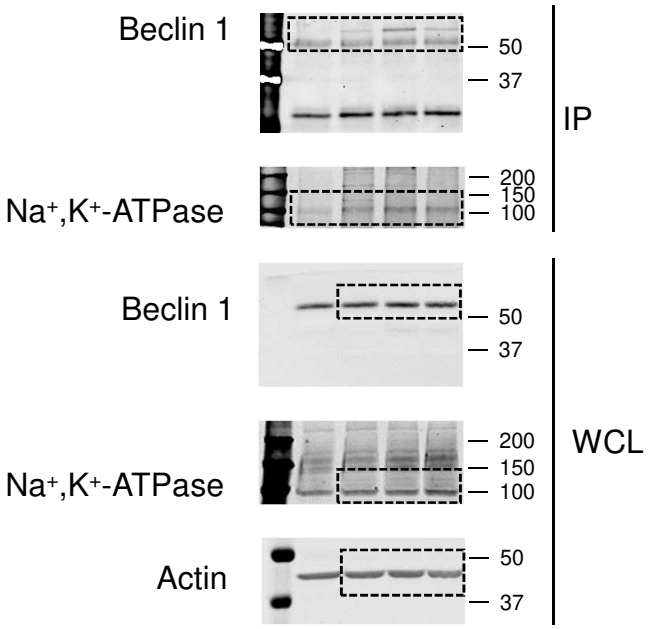

Full unedited gels for Figure 3E

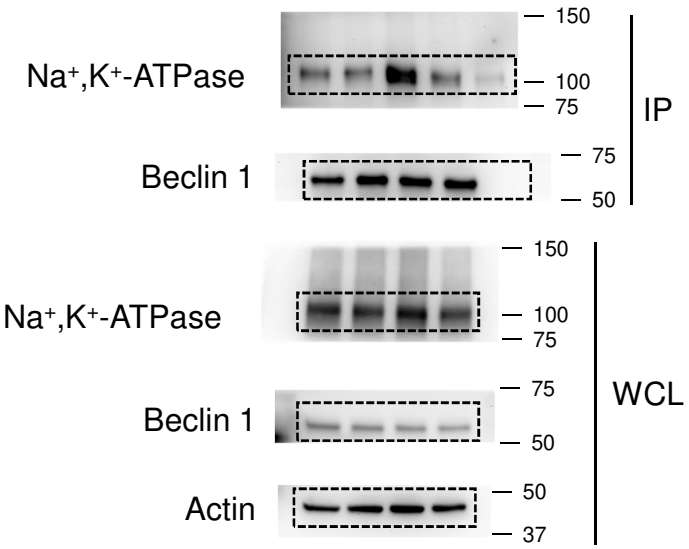

Full unedited gels for Figure 5A

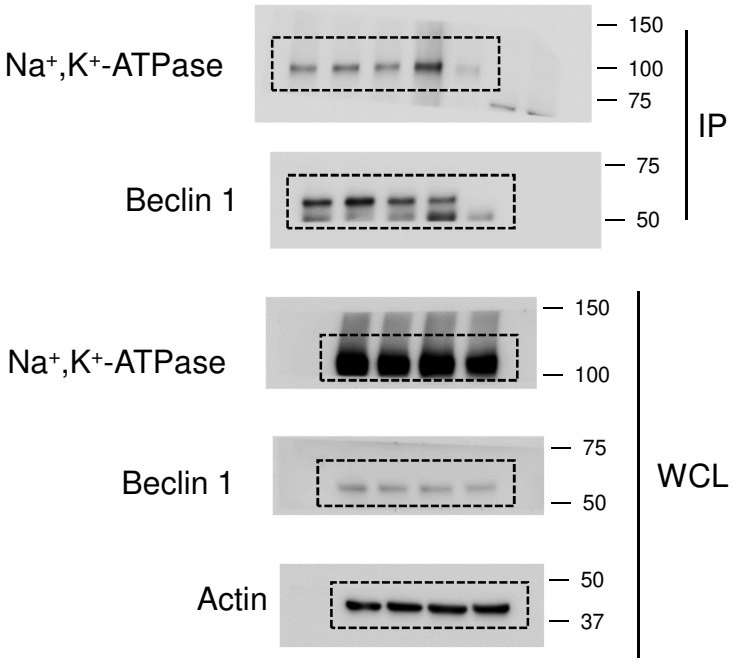

Full unedited gels for Supplemental Figure 2A